

Recent Advances in the Estimation of Extreme Precipitation and Extreme Floods – A Physics-based Perspective

M. L. Kavvas and Y. Iseri
Hydrologic Research Laboratory
Department of Civil & Environmental Engineering
University of California, Davis, CA 95616, USA

Approaches to the estimation of extreme floods:

I. Purely statistical approach to the estimation of the extreme flood;

II. Estimation of extreme flood as a result of a rainfall-runoff analysis with input from statistical analysis of extreme precipitation;

III. Conventional Probable Maximum Precipitation/Probable Maximum Flood Estimation;

IV. Estimation of Maximum Flood based on Numerical Modeling of the Critical Atmospheric-Hydrologic Processes

I. Purely statistical approach to the estimation of the extreme flood based on available historical hydrologic data:

A. Methodology based on considering the flood peak discharge as a random variable:

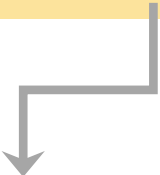
The standard procedure is to construct an empirical frequency histogram

- a) **for the peak discharge of an annual maximum flood event (Gumbel 1941, Dalrymple 1960, Stedinger 1983, Smith J. 1987, WMO 1989, Madsen et al. 1997, Katz et al. 2003, Robson and Reed, 2008, and others), or**
 - b) **of the peak discharge over a specified threshold (WMO 1989, Smith RL 1989, Katz et al. 2003, Robson and Reed 2008, and others) from the available hydrologic data.**
- Extrapolate this histogram to long return periods based on the fit of the empirical frequency histogram by a theoretical probability distribution, such as Log Pearson Type III distribution, Generalized Extreme Value Distribution, Gumbel's distribution, etc.
 - Then estimate the extreme flood discharge for a specified return period from the theoretical probability distribution tail.

I. Purely statistical approach to the estimation of the extreme flood based on available historical hydrologic data:

B. Methodology that considers flood peaks as a stochastic process:

- This approach is mainly based on Peaks over a Threshold (POT) framework.
- After specifying a threshold, the flood peak discharge occurrences above that threshold are modeled as a point stochastic process, either as:

- 
- a Poisson process (Todorovic and Zelenhasic, 1970; RL Smith, 1989 and others) that assumes flood peak occurrences are mutually independent, or
 - a Poisson Cluster process (Cervantes et al. 1983).

II. Estimation of the extreme flood based on a rainfall-runoff simulation with input from extreme precipitation that is estimated by statistical approaches

- i. Development of **frequency curves for extreme precipitation** (probable maximum precipitation), considered as a random variable, based on historical data for specified durations;

This approach, popularized by Herschfield (1961, 1965), develops estimates of maximum precipitation depths as function of geographical location and precipitation duration. It is based on the frequency factor formulation of Ven-Te-Chow (1951). Recent improvements to this estimation procedure were provided by various authors (Koutsoyiannis 1999, Papalexiou and Koutsoyiannis 2013, Nerantzaki and Papalexiou 2021).

- ii. Development of a **Stochastic Weather Generator (WG)** for the time series of precipitation and other atmospheric variables correlated with precipitation;

A WG produces synthetic time series of weather data for a location based on the statistical characteristics of observed weather at that location (Hutchinson 1987, Richardson 1991). The first step in the development of a WG is to model daily precipitation in terms of a Markov Chain or an alternating Renewal Process. The second step is to model the remaining weather variables of interest (temperature, solar radiation, humidity and windspeed, etc.) conditional on precipitation occurrence.

II. Estimation of the extreme flood based on a rainfall-runoff simulation with input from extreme precipitation that is estimated by statistical approaches

iii. Modeling of precipitation by stochastic models;

In this approach precipitation is modeled in terms of the occurrence times of precipitation events above a prespecified threshold as a stochastic point process which are then marked by precipitation depths (Todorovic 1979, Cervantes et al. 1983, Waymire et al. 1984, Smith 1989, Rodrigues-Iturbe et al. 1988, Kavvas et al. 1988, Cowpertwait 1998 and others).

iv. Modeling precipitation random fields by fractals;

In this approach the precipitation fields are analyzed and modeled as fractal or multifractal fields to accommodate their time-space scaling (Schertzer and Lovejoy 1987, Gupta and Waymire 1993, Lovejoy and de Lima 2015, and others).

v. Modeling extreme precipitation by statistical storm transposition;

In this approach the historical precipitation field spatial shape is approximated by a certain geometric shape (circular or elliptical) and the centroid of the approximate field is transposed according to a probability distribution (Gupta 1972, Foufoula-Georgiou 1989). Then by means of the probability distribution of the storm centroid an ensemble of precipitation fields are generated, from which one can obtain basin precipitation depths corresponding to specified return periods. However, this method of historical storm transposition does not conserve the mass, momentum or energy of the historical storm system. Also, the uncertainty in the storm centroid location is different than the chronological uncertainty.

After the precipitation fields are simulated by one of the above approaches, they can then be input to a rainfall-runoff model to produce a corresponding streamflow event that will correspond to the precipitation field of a specified return period.

ISSUES WITH THE ABOVE STATISTICAL APPROACHES

- 1.** None of the above statistical methods for estimating precipitation or floods are physically-based in that they do not conserve neither the mass, nor the momentum nor the energy in the historical storm systems.
- 2.** All of the above methods, except those studies that address the precipitation-flood events as clusters, consider the extreme flood event as a single event with a single extreme peak discharge, although some early studies (WMO 1989) did stress the importance of treating floods as a sequence of events. However, clustering of the flood events as a sequence of inflows to a dam create the most critical conditions for the failure of the dam.
- 3.** Those stochastic Poisson cluster models that address precipitation as a clustered process, do not address the modeling of the floods resulting from these precipitation field clusters.
- 4.** None of the above statistical approaches differentiate and model explicitly the floods with respect to different storm mechanisms (such as floods from atmospheric rivers, floods from extratropical cyclonic systems, floods from mesoscale convective systems, floods from tropical cyclones/hurricanes/typhoons, etc.). However, flood events may behave very differently under different severe storm mechanisms.
- 5.** None of the statistical methods produces realistic spatial configurations of the extreme precipitation fields which vary drastically with different storm mechanisms.

Conventional Method for Estimating Probable Maximum Precipitation (PMP) and Probable Maximum Flood (Paulhus and Gilman 1953, Hansen et al. 1977, Schreiner et al. 1978, WMO 1989, 2009, and various Hydrometeorological Reports of US NWS):

Definition of PMP and PMF (World Meteorological Organization (WMO), 2009)

- Probable Maximum Precipitation (PMP) is defined as the theoretical maximum precipitation for a given duration under possible meteorological conditions.
- Probable Maximum Flood (PMF) is the theoretical maximum flood due to a PMP at a specified river basin or geographical location (such as the inflow location of a dam, or the location of a bridge, etc.).

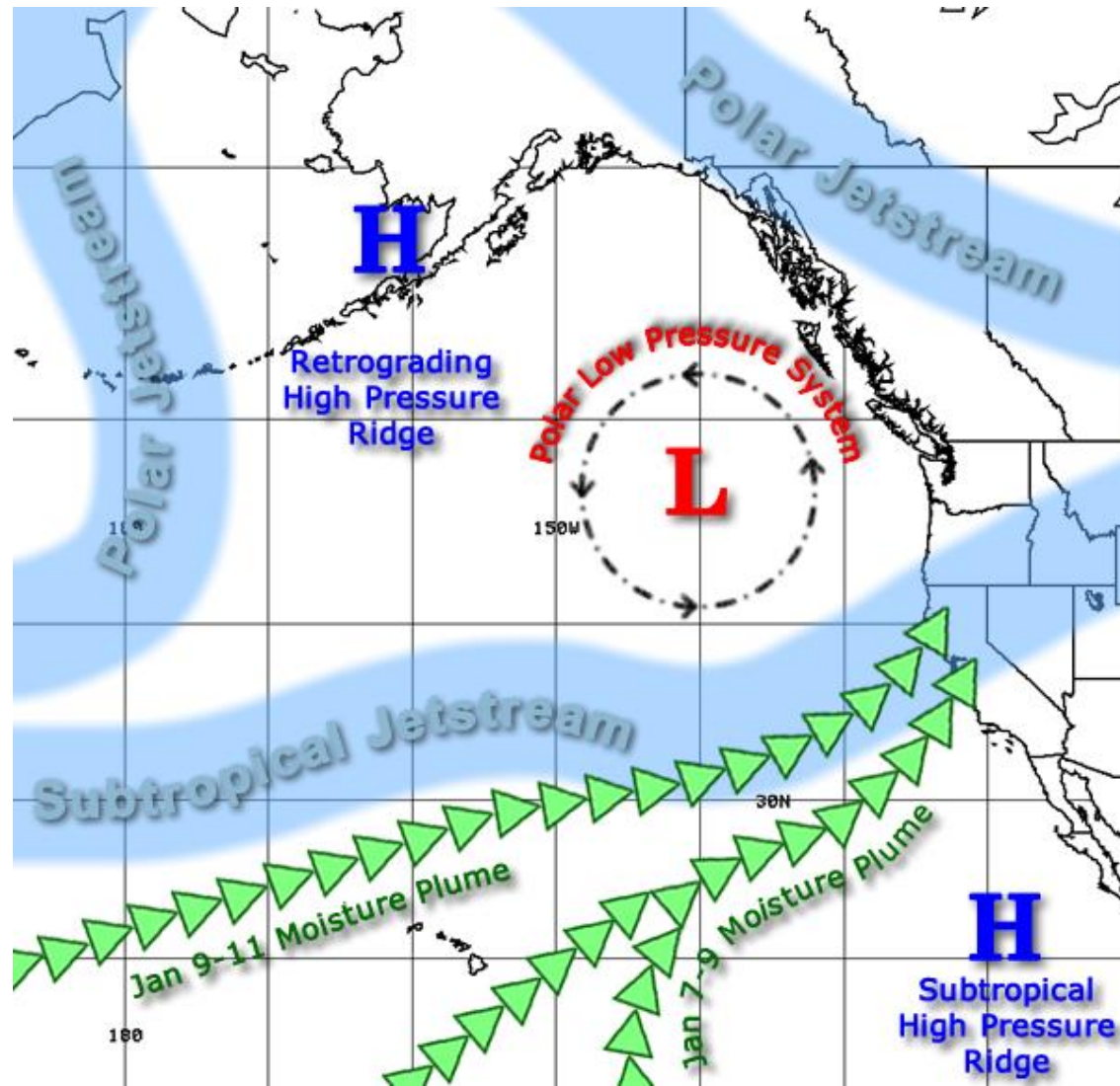
Conventional PMP estimation procedure (WMO, 2009):

- i. Select the historical representative severe storm event;
- ii. Compute the Depth-Area-Duration curves for the selected storm;
- iii. Separate the convergence part of the storm from its orographic component;
- iv. Maximize the moisture in the convergence component of the storm with respect to precipitable water,
- v. Transpose this maximized storm component virtually in order to maximize the precipitation over the target watershed;
- vi. Adjust the estimate for the orographic component (elevation and barrier adjustment); adjust the estimate with respect to duration and area.

Approximations of the Conventional Method for Estimating PMP:

1. The Conventional PMP estimation method artificially separates a storm into non-orographic (convergence) and orographic components while in reality a storm system is a whole that cannot be separated into such components;
2. Precipitation is taken proportional to precipitable water, ignoring the contribution of the moisture flux;
3. The storm transposition is performed virtually, not actually, by adjusting certain storm characteristics;
4. The conservation of mass, momentum and energy of a storm system are not ensured in the storm maximization operations of the Conventional PMP.

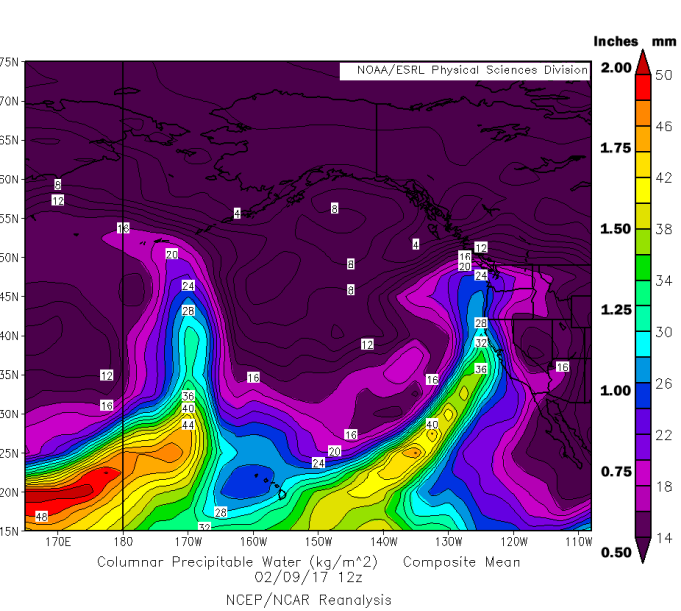
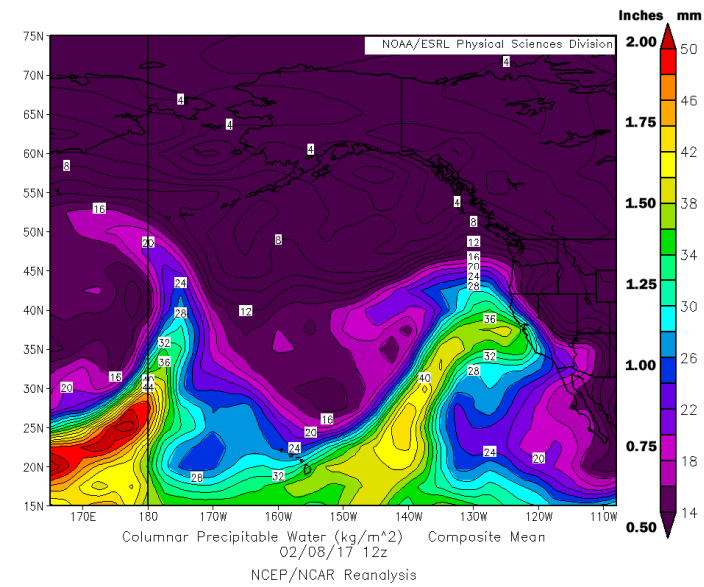
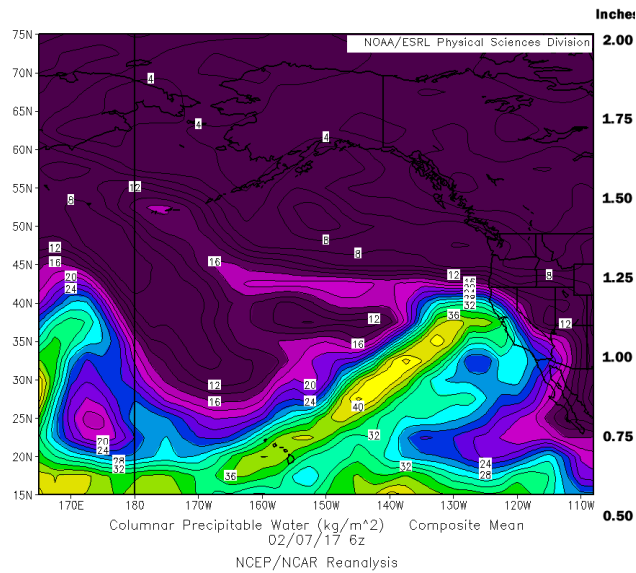
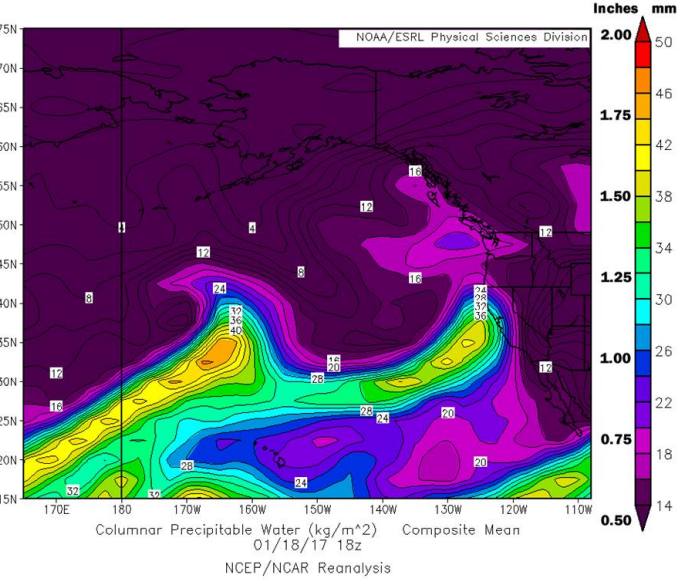
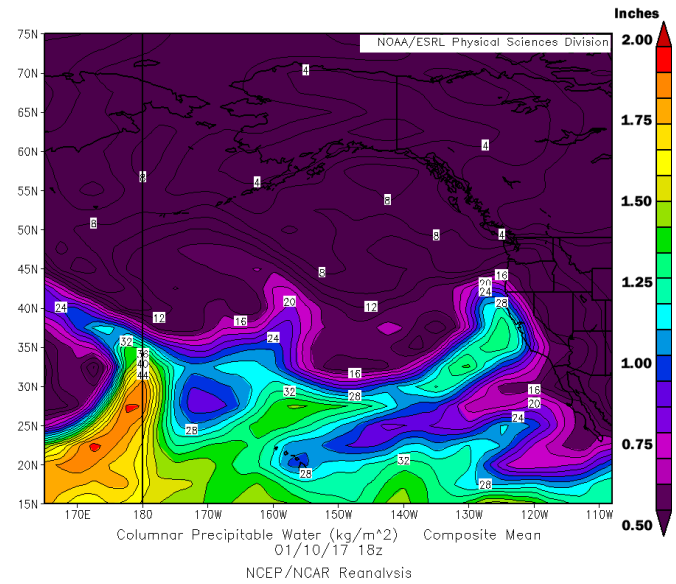
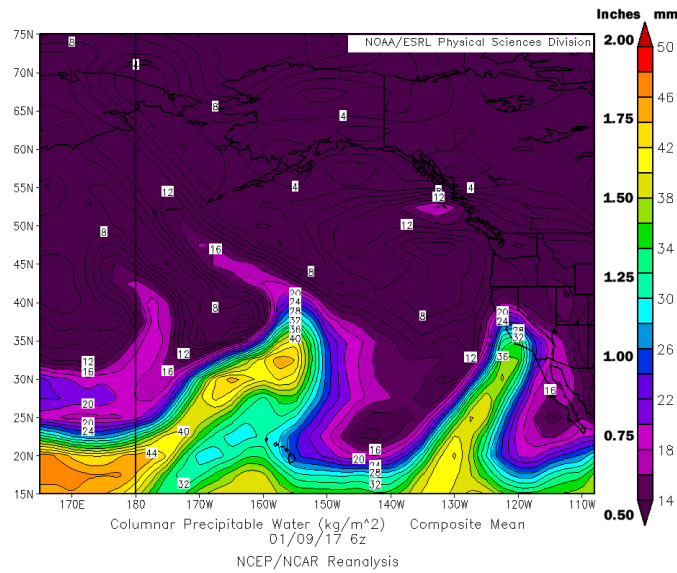
JANUARY 1 – FEBRUARY 28, 2017 SEVERE STORM AND FLOOD OVER CALIFORNIA



General weather pattern across the Eastern Pacific Ocean and West Coast for each storm period during January and February 2017 (CNRFC, 2017).

Atmospheric River

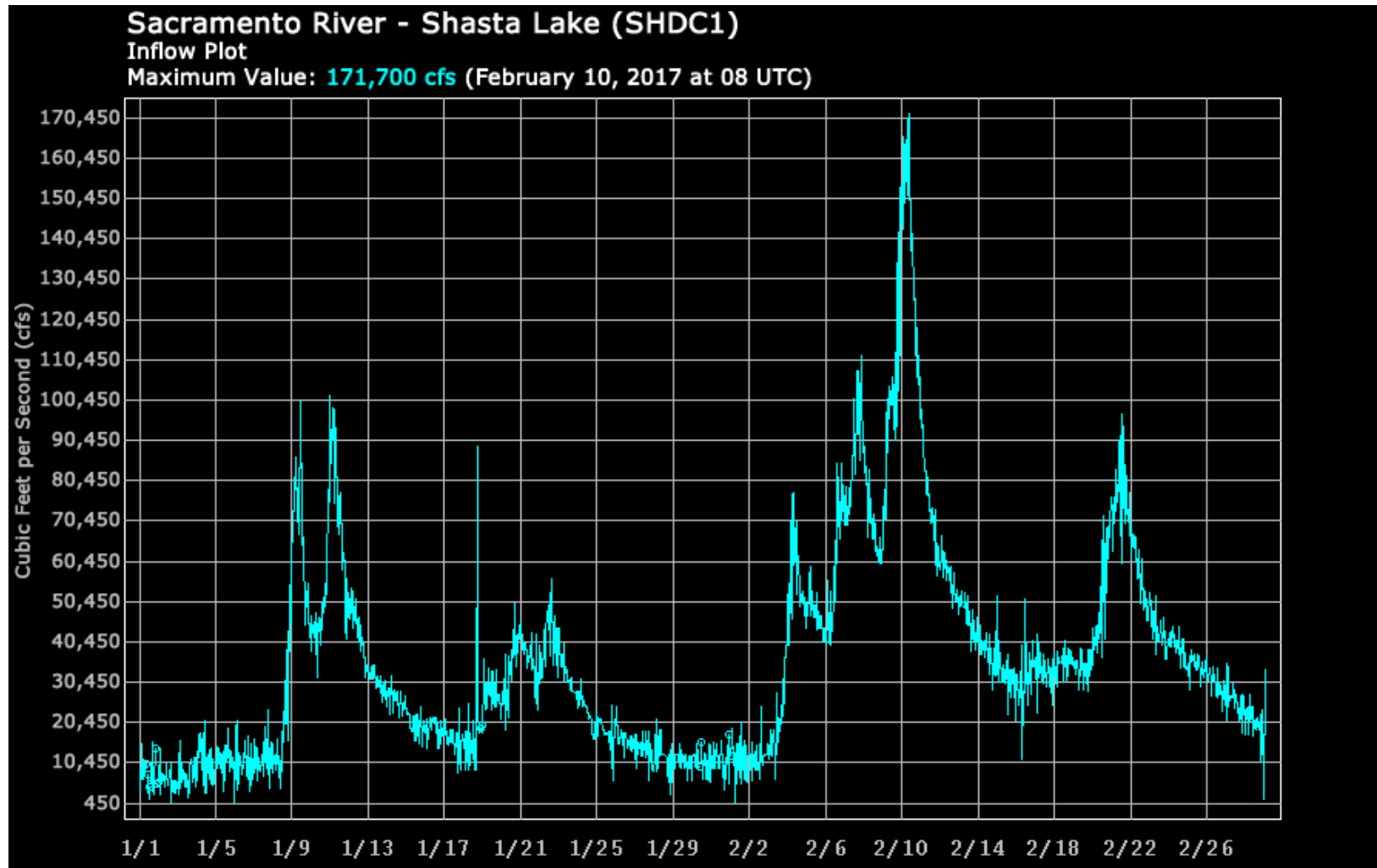
In the west coast of US, severe storms are mainly caused by a high-moisture atmospheric flow coming from a tropical zone of the Pacific Ocean, and referred to as “atmospheric river (AR)”.



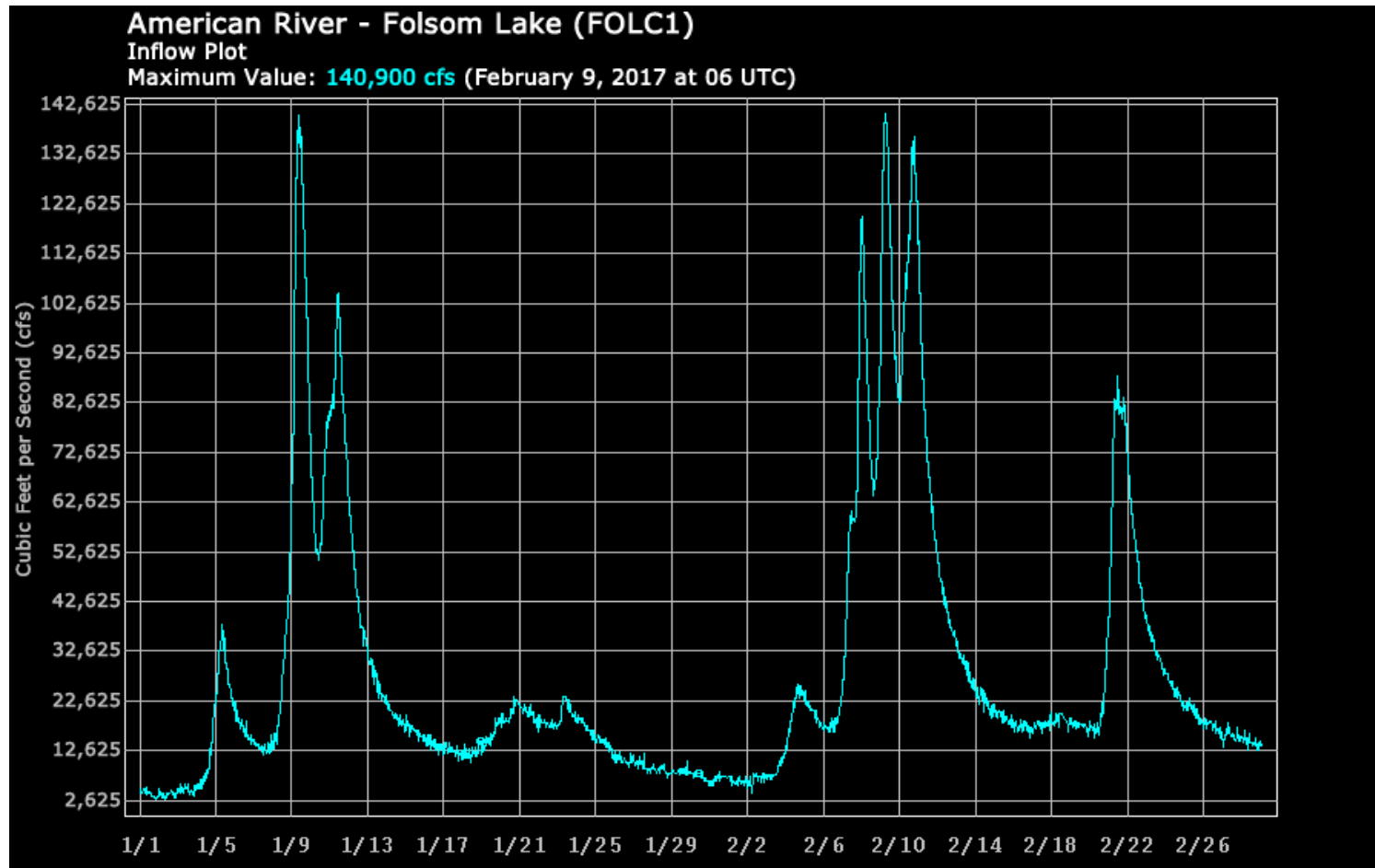
Precipitable Water Fields over the Pacific Ocean near the coast of California on January-February, 2017 California Flood



California River Network System and River Basins



Inflow hydrograph to Shasta Lake during January 1 – February 28, 2017 Flood at Shasta Lake Watershed in California



Inflow to Folsom Lake at American River Watershed, California during the January 1 – February 28, 2017 Flood

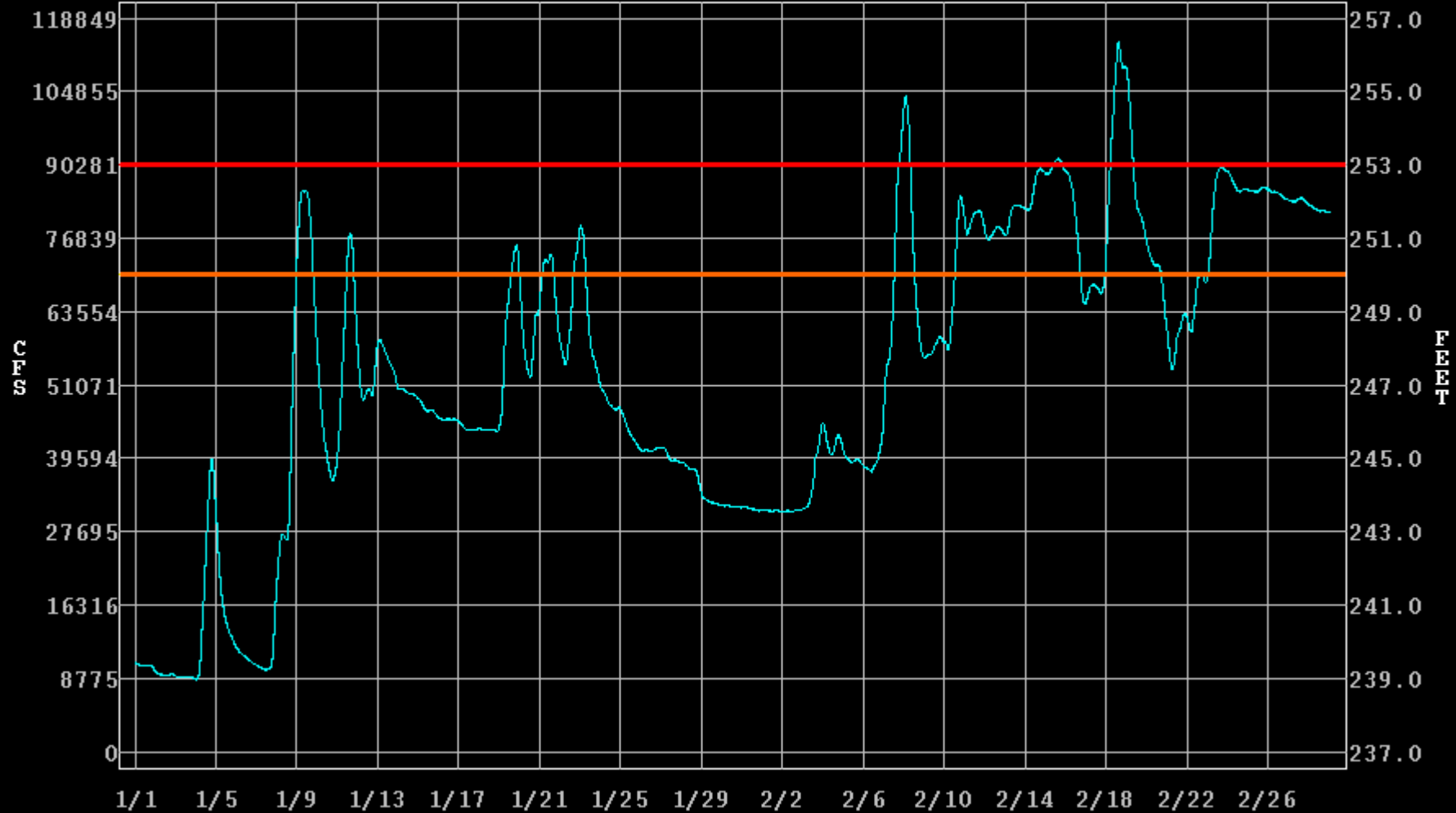
Sacramento River - Red Bluff (RDBC1)

River Stage / Flow Plot

Maximum Value: 256.4 Feet / 114,232 cfs (February 18, 2017 at 14 UTC)

Monitor Stage: 250.0 Feet

Flood Stage: 253.0 Feet



In considering maximum precipitation in the Western Coastal region of the US,

It is critical to consider **how to maximize precipitation caused by the Atmospheric River (AR).**



Development of physically-based method to maximize precipitation caused by ARs.

Precipitation Maximization by a Numerical Atmospheric Model for Atmospheric River (AR) Storm Systems

- I. Select the historical severe storm events from the reconstructed historical precipitation record at a target watershed
 - ✓ Identify the ARs that hit the specified watershed during each of the selected historical severe storm events.

II. Perturbation of the atmospheric fields for the selected historical severe storm events.

II-1. Atmospheric Boundary Condition Shifting

II-2. Relative humidity optimization

III. Probable Maximum Precipitation (PMP) over a target watershed

I. Select the historical severe storm events from the reconstructed historical precipitation record at a target watershed;

Limitations in using observed precipitation data;

- The number of observation stations in a target study area and their recording periods are insufficient.
- The PRISM daily data set (Daly et al. 2008, 2013) covers the continental US for the period 1981 to present at 4 km grid resolution (PRISM Climate Group, 2016).
- Many of the recorded historical floods over a target watershed may have happened prior to 1981.

Meanwhile, there are various historical atmospheric reanalysis data sets some of whom date as far back as to 1851.

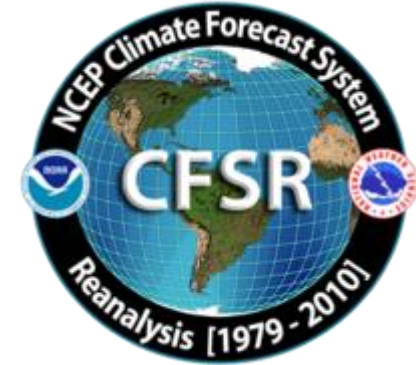
Global Reanalysis data



NOAA/CIRES 20th Century
Reanalysis (20CR) Version 2c
- 1851 – 2014
- Horizontal resolution of 2
degree (T62), 24 vertical levels



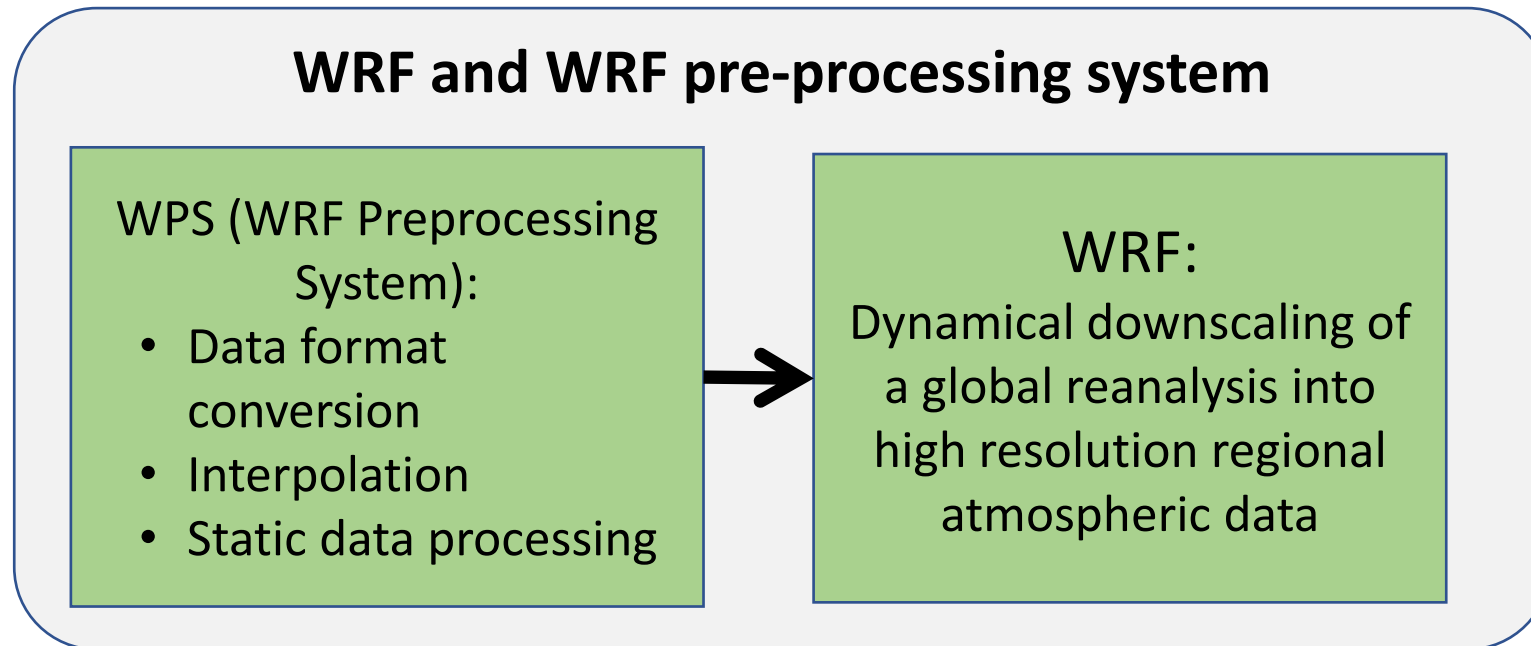
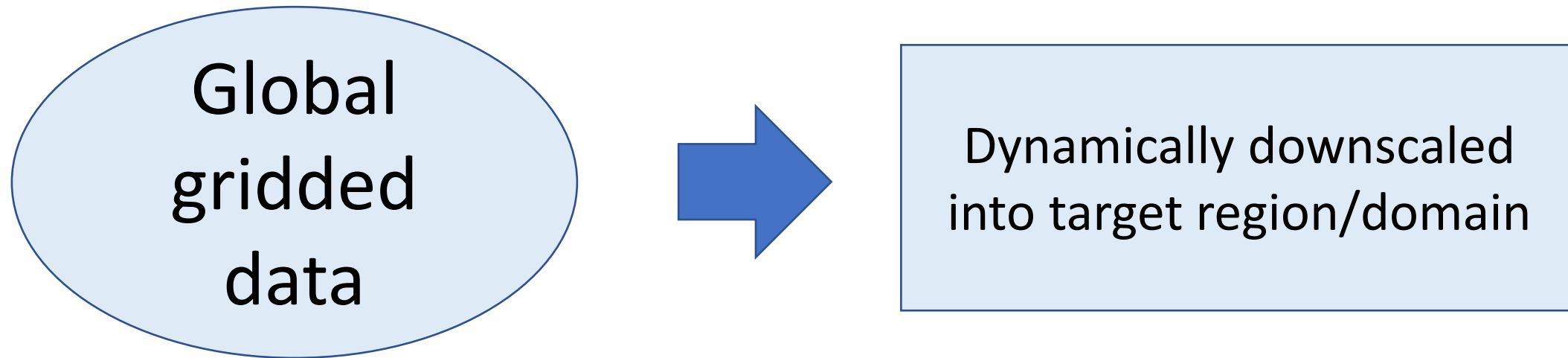
ECMWF Twentieth Century
Reanalysis (ERA-20C)
- 1900 – 2010
- Horizontal resolution of 125 km
(T159), 37 vertical levels



NCEP Climate Forecast System
Reanalysis (CFSR)
- 1979 – 2016
- Horizontal resolution of 0.5
degree (T382), 64 vertical levels

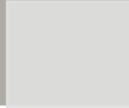
- Reconstruction of the historical atmospheric conditions over any target watershed over the world can be performed by means of reanalysis global data sets that are available from various atmospheric organizations around the world, such as US NCAR, ECMWF, etc.
- Hence, it is necessary to reconstruct the historical atmospheric conditions at hourly or finer intervals by a numerical atmospheric model after the model is calibrated and validated by the available PRISM daily data.

Weather Research & Forecasting model (WRF)




I. Select the historical severe storm events from the reconstructed historical precipitation record at a target watershed

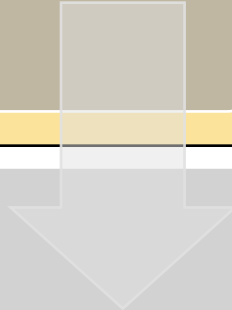
Use a numerical atmospheric model (WRF) to reconstruct atmospheric fields;



Choose the most severe historical storms based on the moisture conditions in these storms (such as precipitation depth or maximum IVT exceeding a specified threshold during the storm duration);



Shift the atmospheric fields so that the atmospheric river strikes the target watershed at the optimal location and in the optimal direction to produce the maximum precipitation over the watershed.



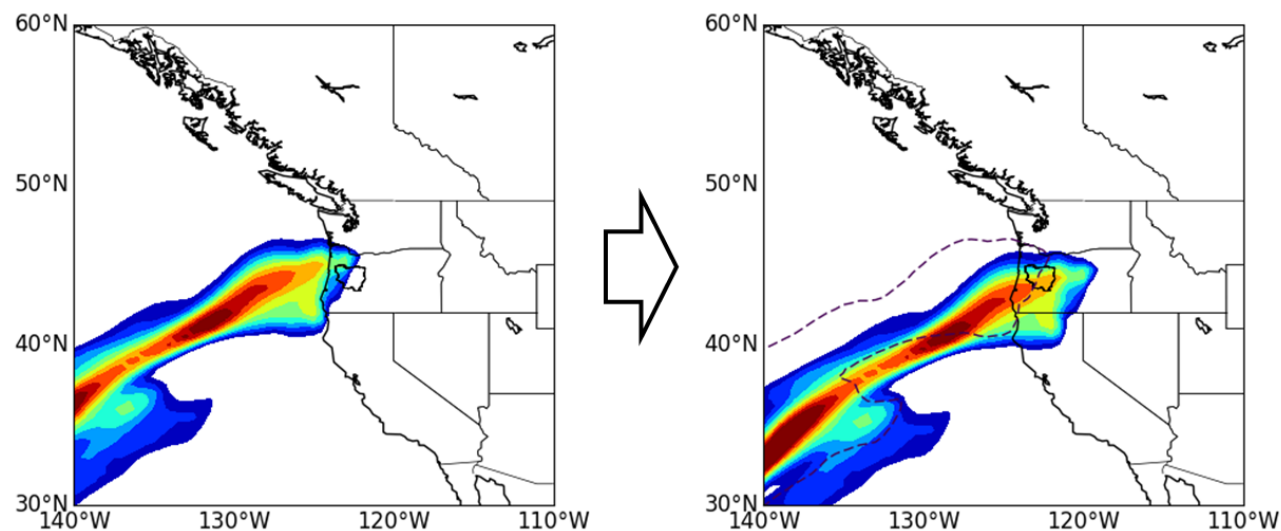
II. Perturbation of the atmospheric fields for the selected historical severe storm events.

II-1. Atmospheric Boundary Condition Shifting Method

1. Shift the atmospheric BCs with respect to only latitude (Shift1D) and then also with longitude (Shift2D) (Ohara et al. 2011, Ishida et al. 2015);
2. Shift the atmospheric BCs along an identified AR until the basin-average precipitation reaches a maximum and then starts to decrease.

Differences from traditional PMP Approach

- Uses a physically-based numerical atmospheric model
- Produces all relevant atmospheric variables' information for a given severe storm (besides the precipitation, also the wind field, humidity field, temperature field, radiation field, etc. for the specified storm)



II. Perturbation of the atmospheric fields for the selected historical severe storm events.

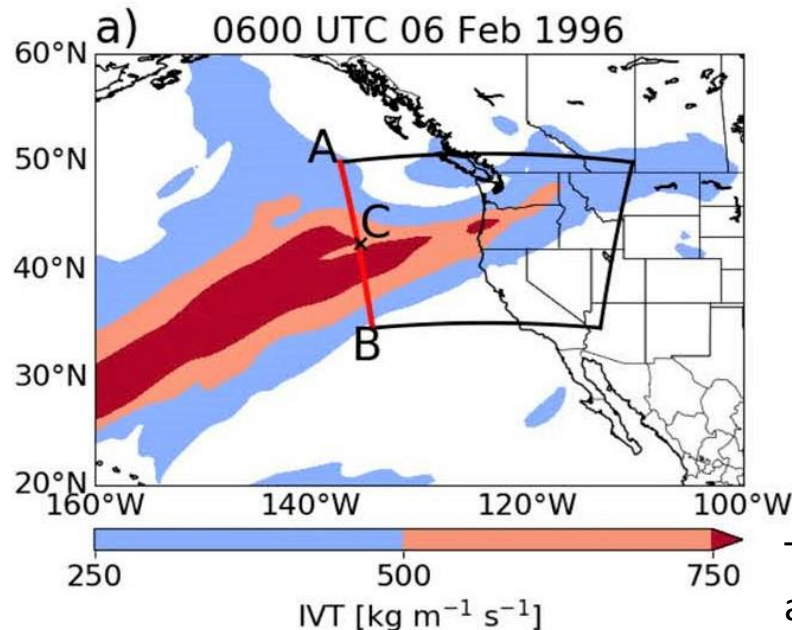
II-2. Relative humidity optimization

The Relative Humidity (RH) perturbation method (RHP-IVT method; Toride et al., 2019) increases RH proportionally at those boundary sections where high IVT values are observed in order to maximize the storm event with physically realistic atmospheric fields.

$$IVT = \frac{1}{g} \int_{1000}^{300} \bar{q} \bar{U} dp$$

g : gravitational acceleration ($m s^{-2}$), \bar{q} is the mean layer specific humidity ($kg kg^{-1}$),

\bar{U} : mean layer horizontal wind speed ($m s^{-1}$), p : the pressure (hPa)



Toride et al. 2019

Left:

Example of moisture perturbation along the path of an atmospheric river: a) Integrated water vapor transport (IVT) in [$kg/m\text{-sec}$] at 0600 UTC 6 Feb 1996. The black box shows the outer modeling domain.

II. Perturbation of the atmospheric fields for the selected historical severe storm events.

II-2. Relative humidity optimization

$$RH = \begin{cases} \min(\beta RH_0, 97), & \text{if } RH_0 < 97\% \\ RH_0, & \text{if } RH_0 \geq 97\% \end{cases}$$

where RH_0 is the original relative humidity (%) and β is a multiplication factor to determine the increment of RH.

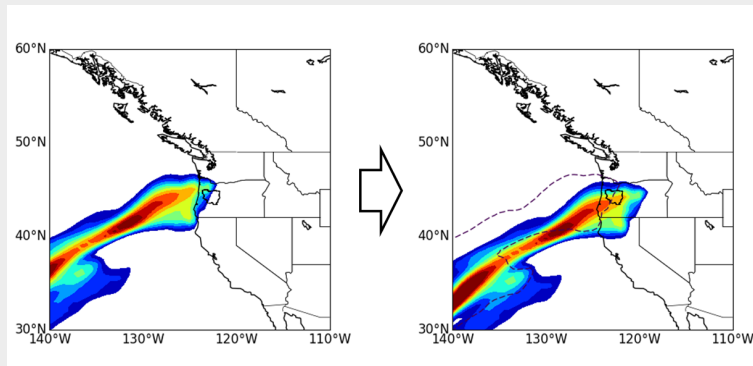
The above equation sets the upper threshold of RH to 97% in order to avoid quick saturation near the modeling boundary (Zhao et al., 1997).

- Relative humidity (over areas where the IVT > 250 kg/m/s) is gradually increased, along with BC shifting until a maximum basin-average precipitation depth is reached.
- 100s of regional atmospheric numerical simulations are performed in order to reach the atmospheric conditions that maximize the basin-average precipitation depth.

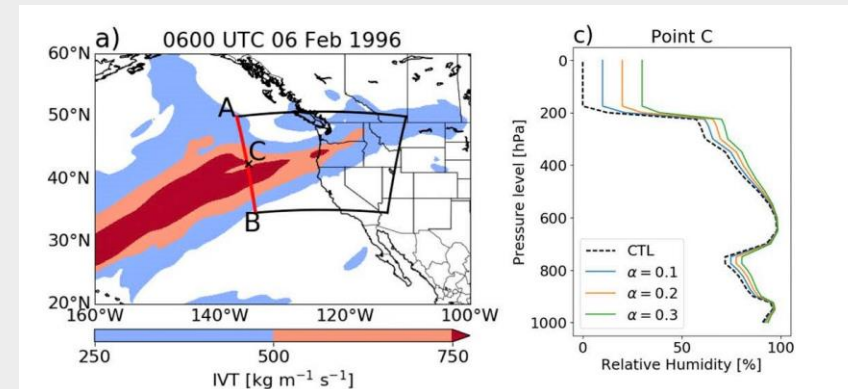
II. Perturbation of the atmospheric fields for the selected historical severe storm events

The reconstructed atmospheric fields for the selected historical severe storm events

II-1. Atmospheric boundary condition shifting



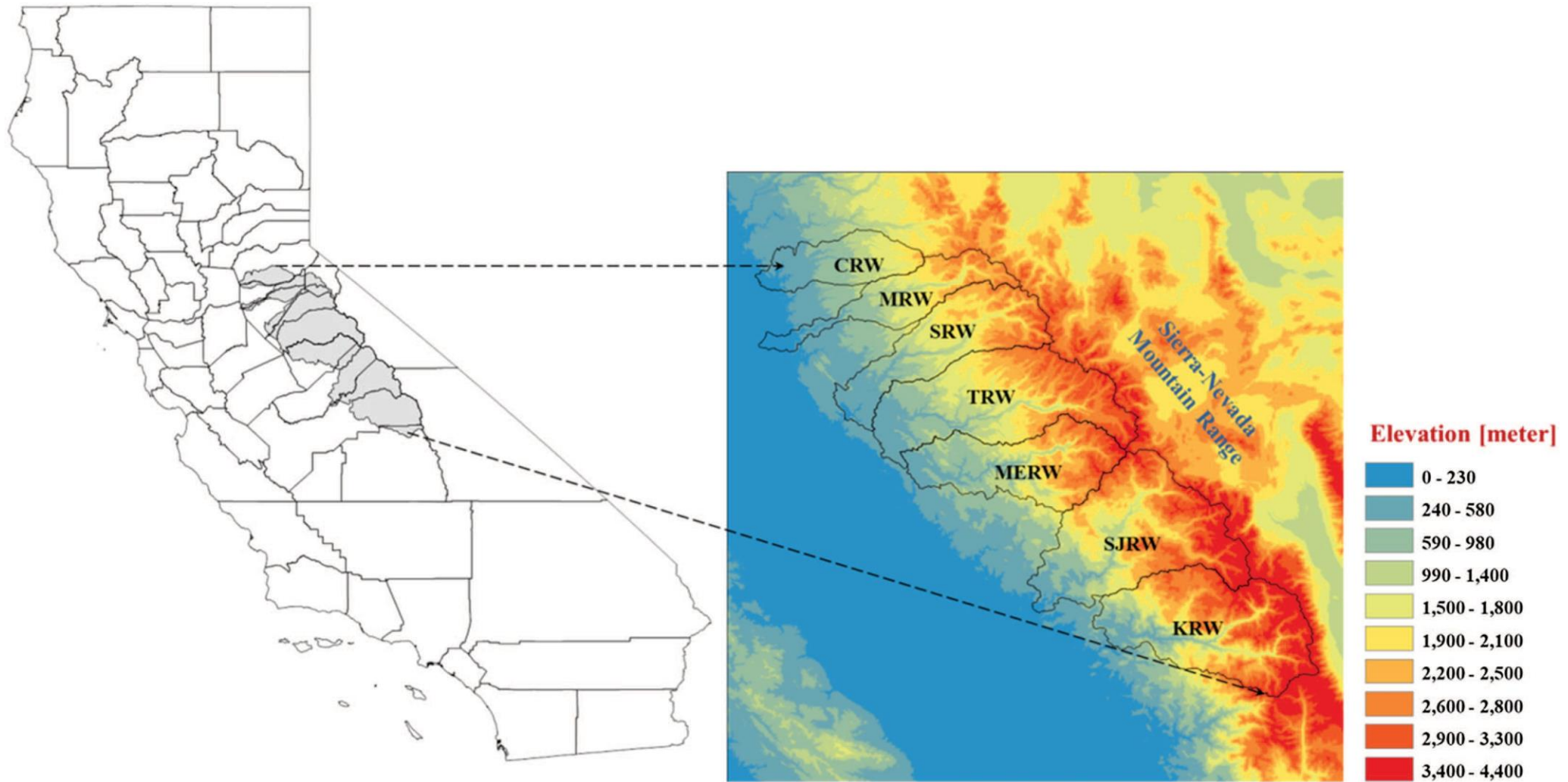
II-2. Relative humidity optimization



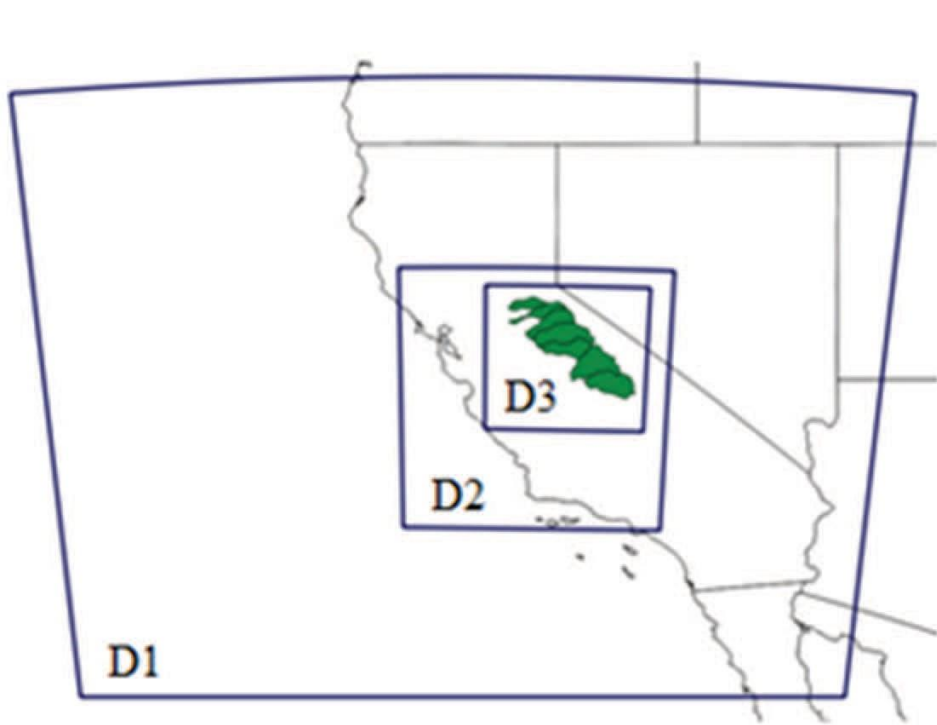
&

III. Probable Maximum Precipitation (PMP) over a target watershed

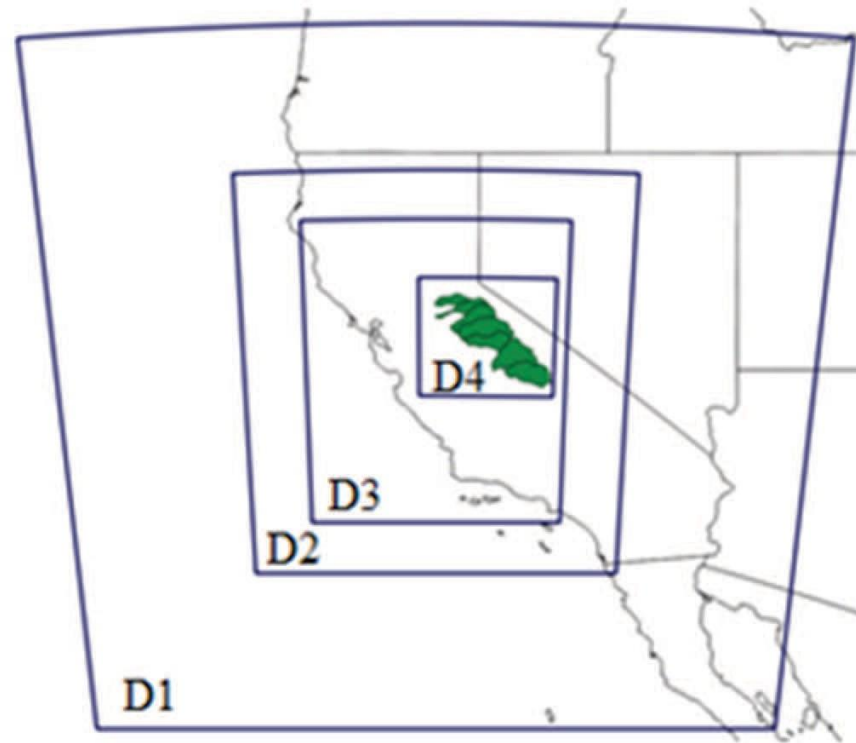
Example of physically-based PMP/PMF
estimation for
Seven Southern California watersheds



Locations and elevation map of the target watersheds, consisting of the Cosumnes (CRW), Mokelumne (MRW), Stanislaus (SRW), Tuolumne (TRW), Merced (MERW), Upper San Joaquin (SJRW), and Upper Kings (KRW).

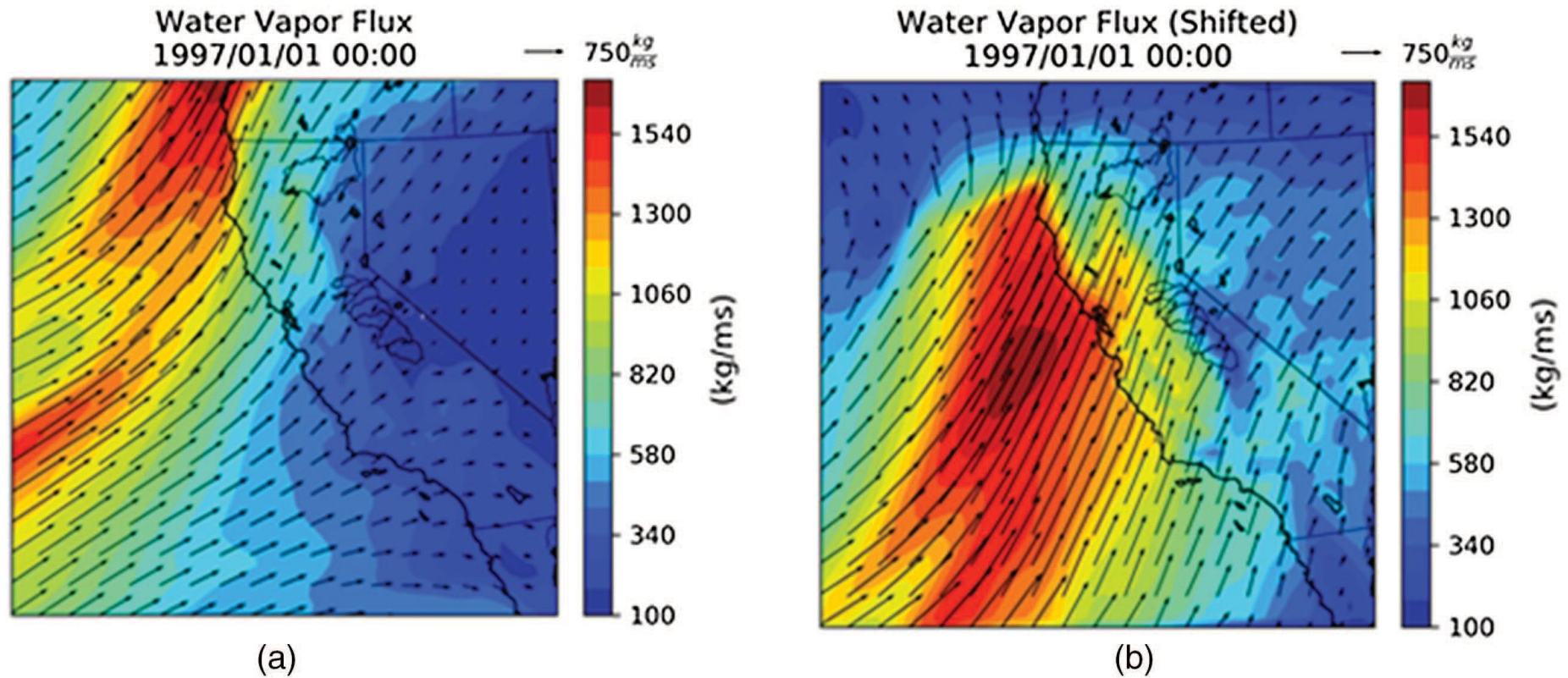


(a)

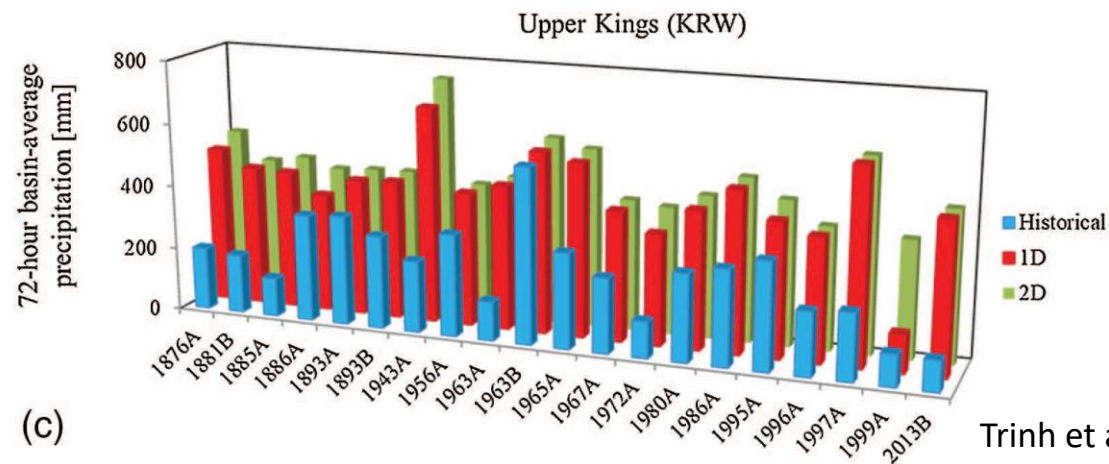
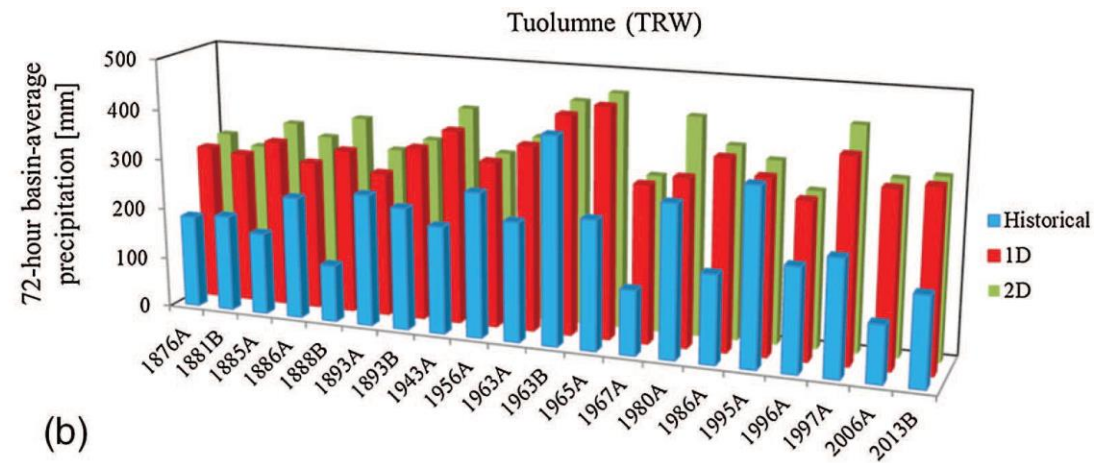
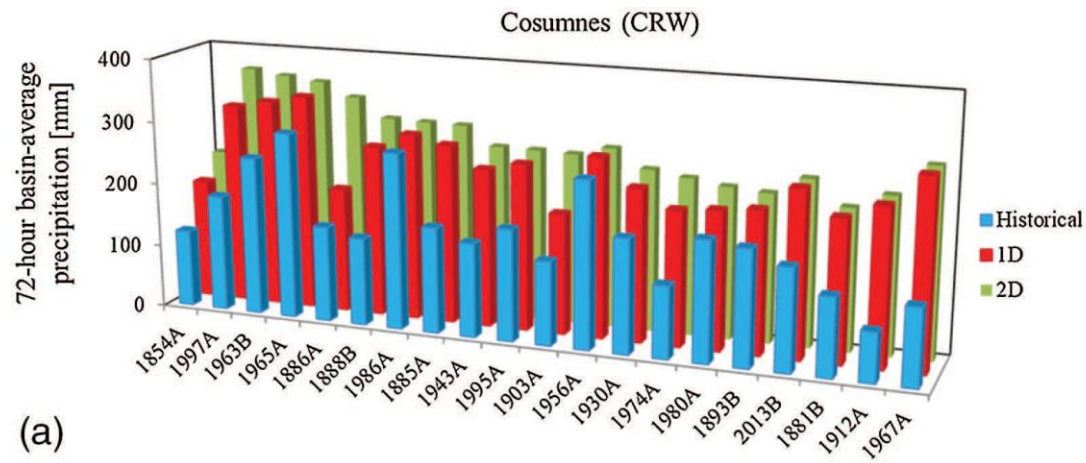


(b)

Nested domains for the WRF simulation used with (a) CFSR reanalysis and ERA-20C data sets; and (b) 20CRv2c reanalysis data set.



Atmospheric River (AR) position based on IVT:
(a) before shifting; and (b) after atmospheric boundary condition shifting.



Trinh et al. (2021)

Top 20 maximized 72-h precipitation (mm) depth events (identified by their dates) for historical reconstruction (blue), 1D maximized 72-h precipitation depth (red), and 2D maximized 72-h precipitation depth (green): (a) Cosumnes (CRW) watershed; (b) Tuolumne (TRW) watershed; and (c) Upper Kings (KRW) watershed

Watershed	Event	Historical precipitation depth (mm)	1D shifting precipitation depth (mm)	2D shifting precipitation depth (mm)	Shift to north (°)	Shift to east (°)
Cosumnes	1997A	183.74	317.05	366.53	-5	1
	1963B	250.22	328.51	359.38	2	1
	1965A	294.17	340.55	353.47	-2	-1
	1886A	150.82	196.66	332.30	5	1
	1888B	138.24	269.62	302.54	-5	1
Mokelumne	1965A	299.59	428.88	428.88	-4	0
	1997A	240.38	377.01	415.46	-5	1
	1963B	339.35	396.00	397.43	2	1
	1963A	160.77	391.32	391.32	-1	0
	1986A	312.30	343.43	361.24	-1	-1
	Stanislaus	1965A	270.07	433.08	439.01	-5
1997A		241.08	410.27	434.75	-5	1
1963B		366.97	402.76	403.31	2	1
1963A		180.49	394.64	394.64	-1	0
1943A		190.41	337.81	368.72	-5	-1

Watershed	Event	Historical precipitation depth (mm)	1D shifting precipitation depth (mm)	2D shifting precipitation depth (mm)	Shift to north (°)	Shift to east (°)
Tuolumne	1965A	253.80	450.16	460.00	-5	1
	1963B	406.24	428.05	440.14	1	1
	1997A	226.64	394.00	433.32	-5	1
	1980A	298.72	327.38	426.68	-5	1
	1943A	211.80	380.75	409.58	-5	-1
	Merced	1965A	214.81	478.16	490.13	-5
1963B		402.18	411.91	411.91	1	0
1943A		191.70	378.77	407.93	-5	-1
1980A		254.42	291.40	403.95	-5	1
1986A		205.71	387.86	402.89	-2	-1
Upper San Joaquin	1943A	224.51	521.43	560.79	-4	-1
	1997A	190.05	494.14	494.14	-5	0
	1965A	253.50	475.13	475.13	-5	0
	1963B	442.29	434.20	465.32	1	1
	1995A	381.82	407.61	429.89	1	1
Upper Kings	1943A	225.72	678.20	745.59	-5	-1
	1963B	551.20	568.44	585.70	0	1
	1997A	209.51	608.97	608.97	-5	0
	1965A	300.17	544.08	560.46	-5	1
	1876A	197.02	490.49	525.53	-5	-1

Top five events after precipitation maximization using ABCS (Atmospheric BC Shifting)

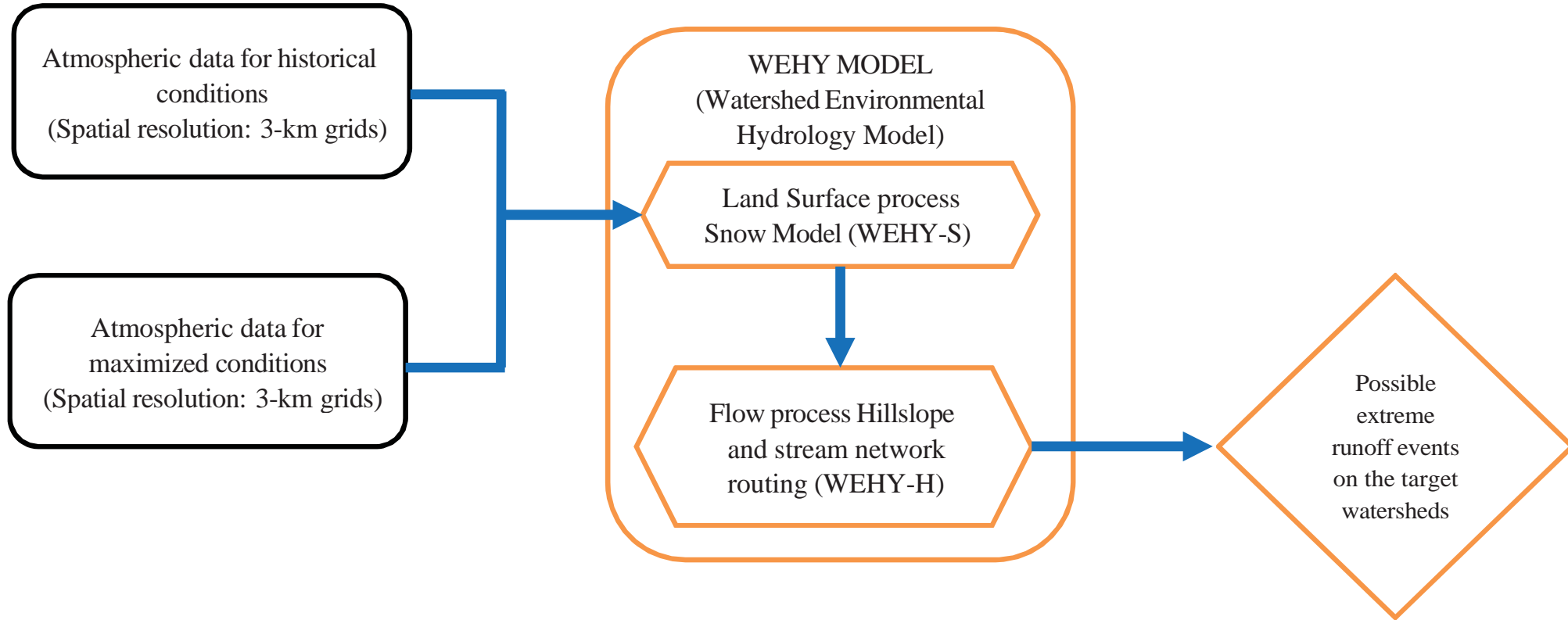
Watershed	Event	Historical precipitation depth (mm)	1D shifting precipitation depth (mm)	2D shifting precipitation depth (mm)	RHP-IVT precipitation depth (mm)	Shift to north (°)	Shift to east (°)	Increase in RHP-IVT (%)
Cosumnes	1965A	294.17	340.55	353.47	424.27	-1	-1	14
	1997A	183.74	317.05	366.53	416.60	-5	-1	18
	1886A	150.82	196.66	332.30	409.28	5	1	20
	1963B	250.22	328.51	359.38	387.87	2	1	12
	1986A	278.06	293.50	300.85	354.48	1	1	12
Mokelumne	1886A	210.24	270.31	306.79	533.44	5	1	20
	1997A	240.38	377.01	415.46	500.77	-5	0	20
	1965A	299.59	428.88	425.99	479.52	-3	0	20
	1963B	339.35	396.00	397.43	452.76	2	1	12
	1885A	172.79	316.61	323.73	365.57	-2	0	14
Stanislaus	1997A	241.08	410.27	434.75	517.49	-5	0	20
	1886A	227.42	284.55	303.74	513.10	5	1	20
	1965A	270.07	433.08	439.01	491.86	-5	-1	20
	1963B	366.97	402.76	403.31	436.79	2	1	12
	1986A	312.58	339.70	347.60	397.97	1	1	20
Tuolumne	1886A	241.13	293.71	330.37	556.09	5	1	20
	1997A	226.64	394.00	433.32	524.71	-5	0	20
	1965A	253.80	450.16	460.00	491.51	-5	1	20
	1963B	406.24	428.05	440.14	477.85	2	1	12
	1980A	298.72	327.38	426.68	427.03	-5	1	20
Merced	1886A	226.21	252.89	300.34	559.41	5	1	20
	1965A	214.81	478.16	490.13	546.11	-5	-1	20
	1997A	162.44	398.35	394.88	491.78	-5	0	20
	1963B	402.18	411.91	410.93	470.92	2	1	12
	1986A	205.71	387.86	402.89	441.69	1	0	16
Upper San Joaquin	1886A	293.53	323.83	376.18	654.31	5	1	20
	1997A	190.05	494.14	488.82	607.81	-5	1	20
	1943A	224.51	521.43	560.79	560.91	-5	-1	10
	1965A	253.50	475.13	472.78	527.72	-5	-1	20
	1963B	442.29	434.20	465.32	494.33	-2	0	20
Upper Kings	1943A	225.72	678.20	745.59	794.26	-5	-1	20
	1997A	209.51	608.97	567.79	723.37	-5	-1	20
	1886A	335.88	371.94	430.53	719.60	5	1	20
	1963B	551.20	568.44	585.70	640.23	-2	0	20
	1965A	300.17	544.08	560.46	626.04	-5	1	20

Top five events after precipitation maximization using RHP-IVT for each watershed

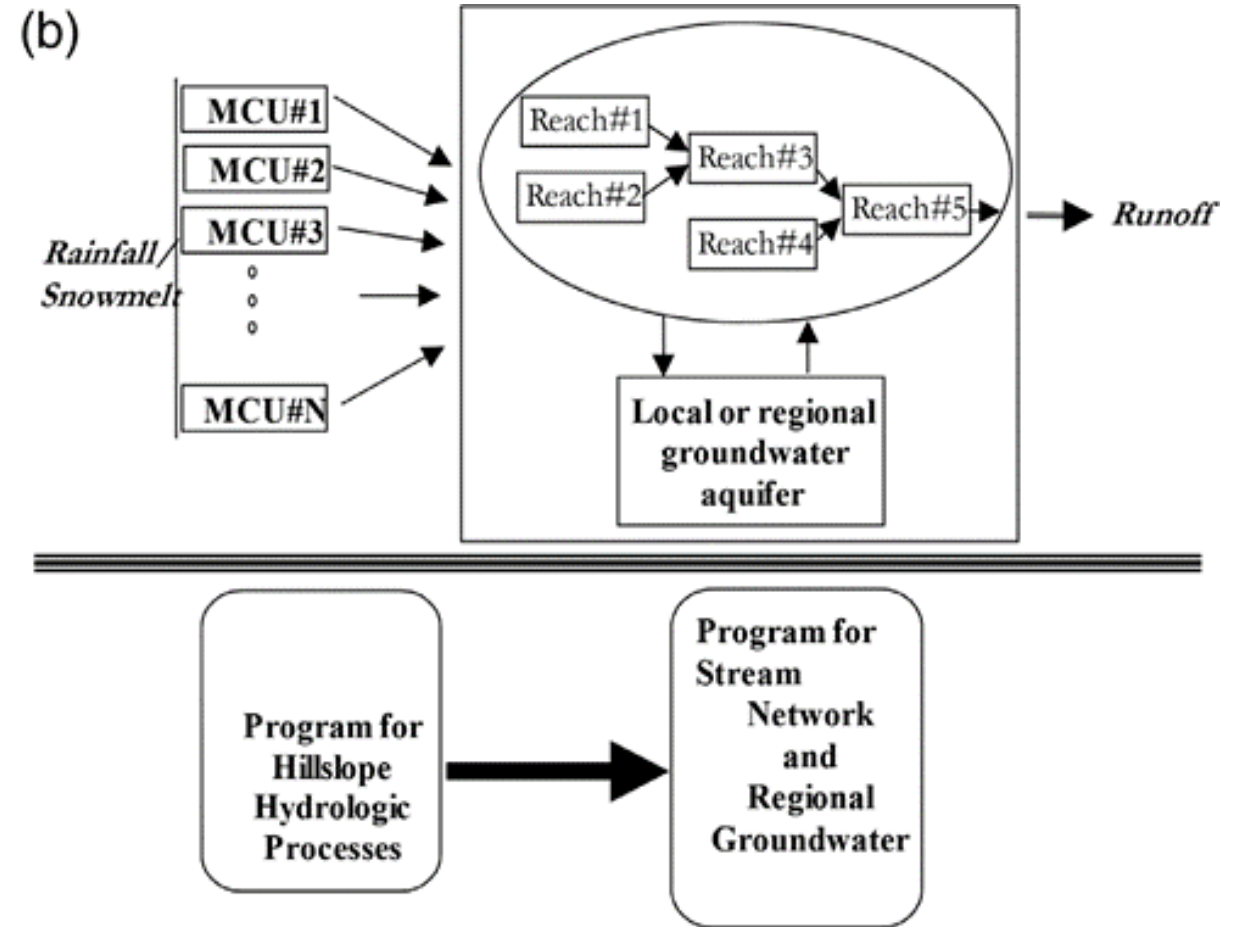
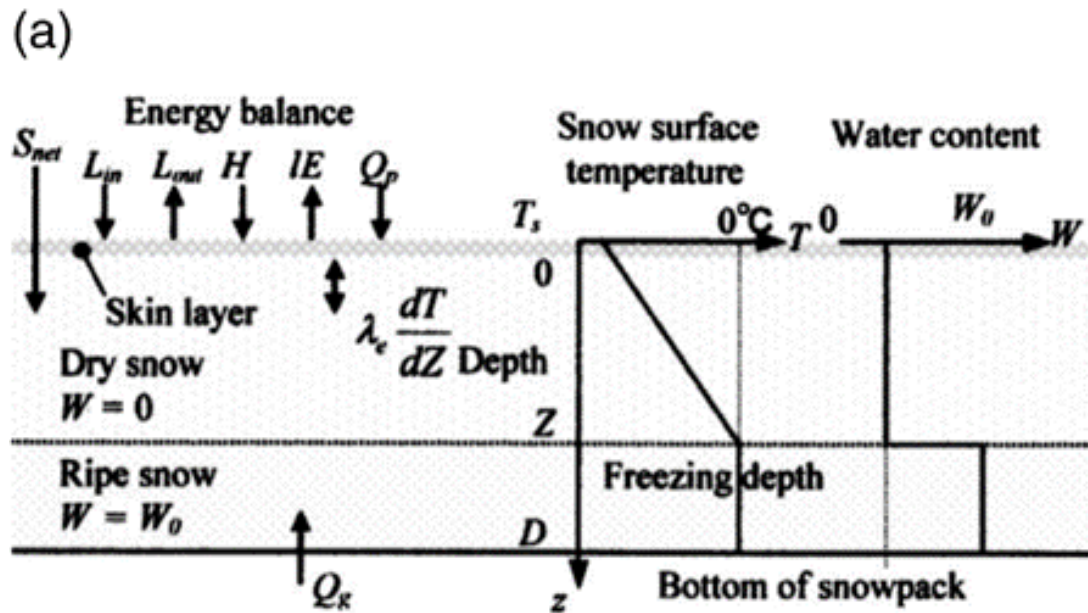
Historical and the maximized atmospheric fields

WEHY (hydrologic model including snow process)

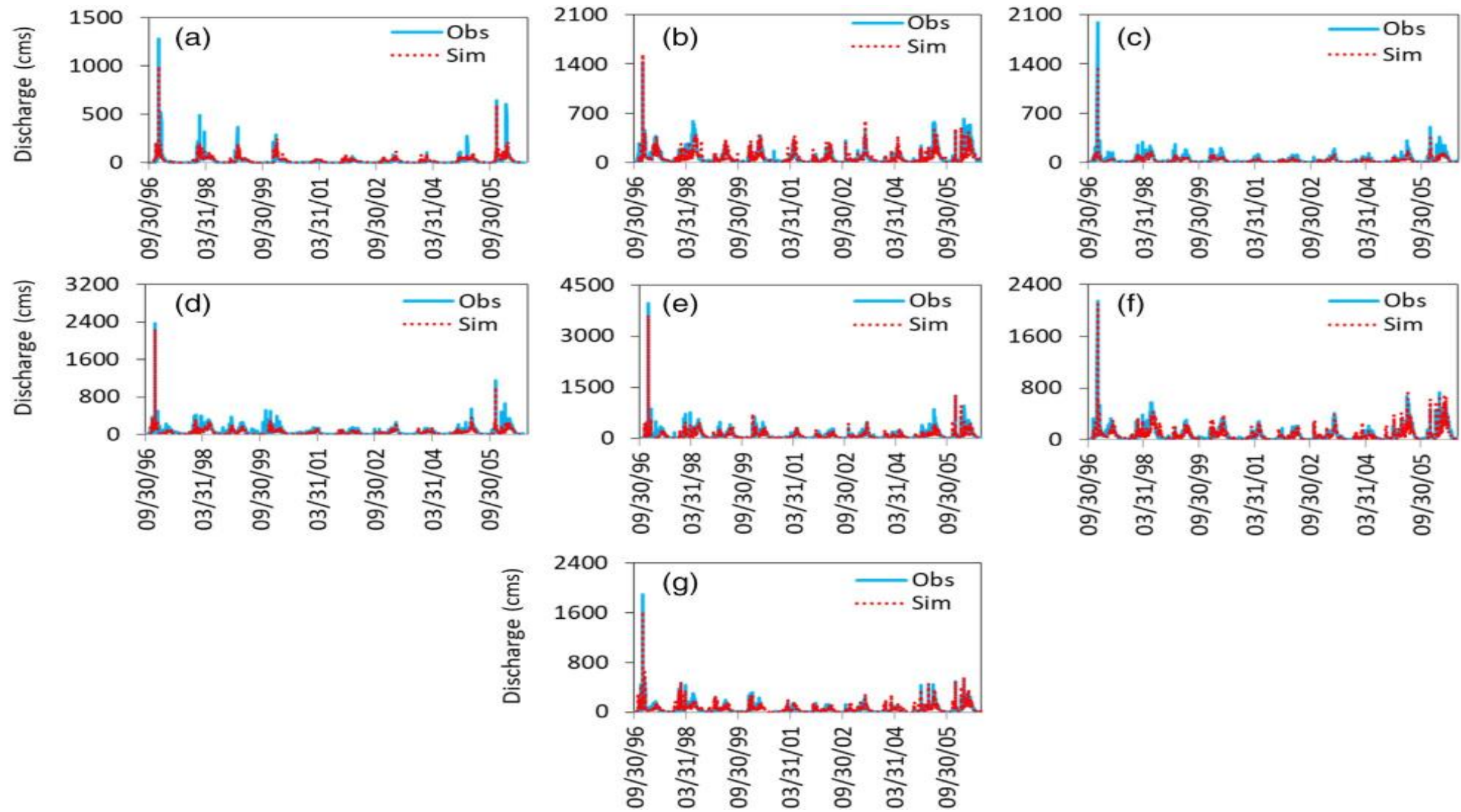
PMF estimation



Schematic description of the proposed methodology to simulate maximum flood events



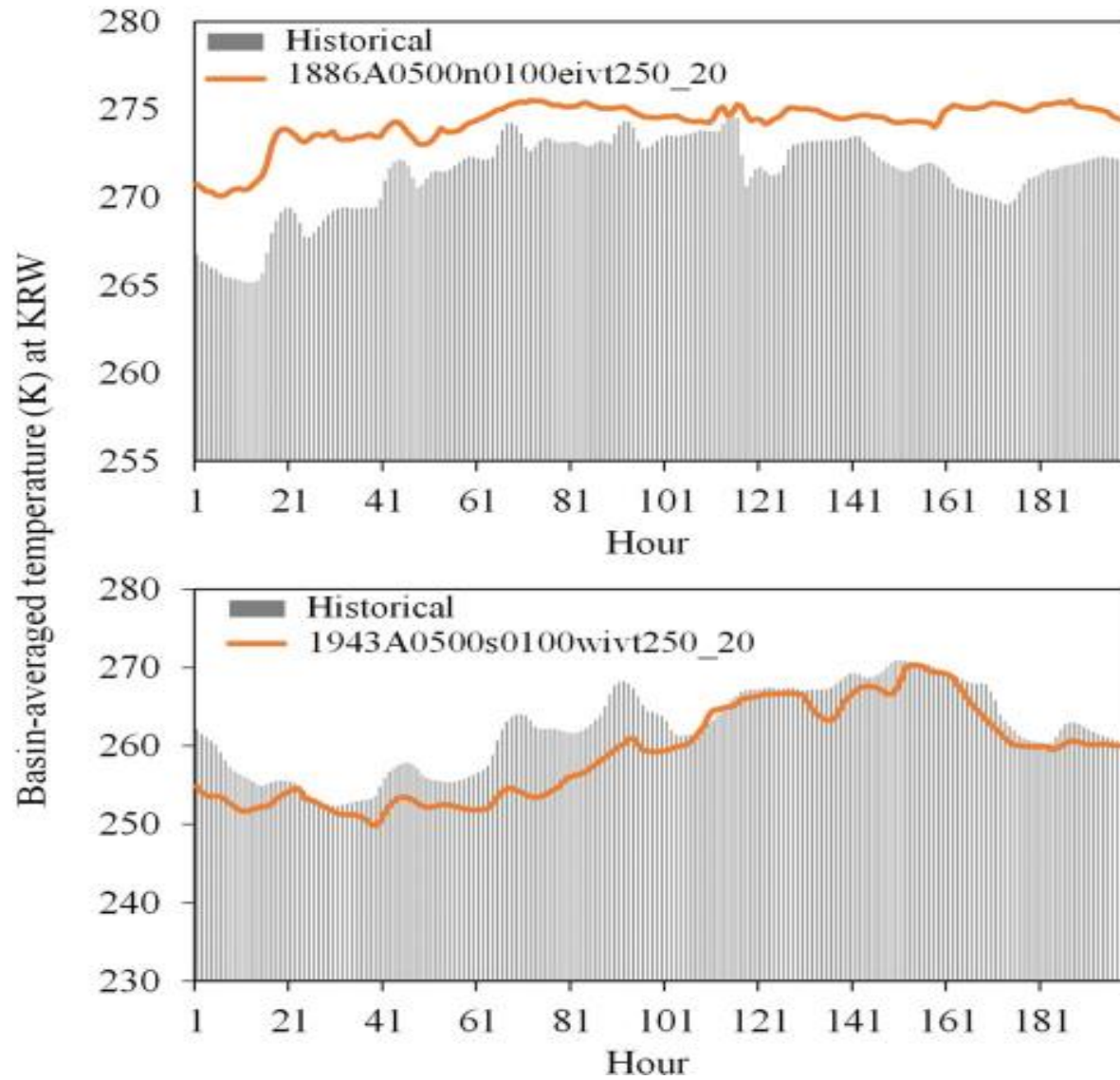
(a) WEHY-S conceptualization of temperature profile, water content profile, and energy balances within and around snowpack; (b) structural description of WEHY-H (Kavvas et al., [2013](#))



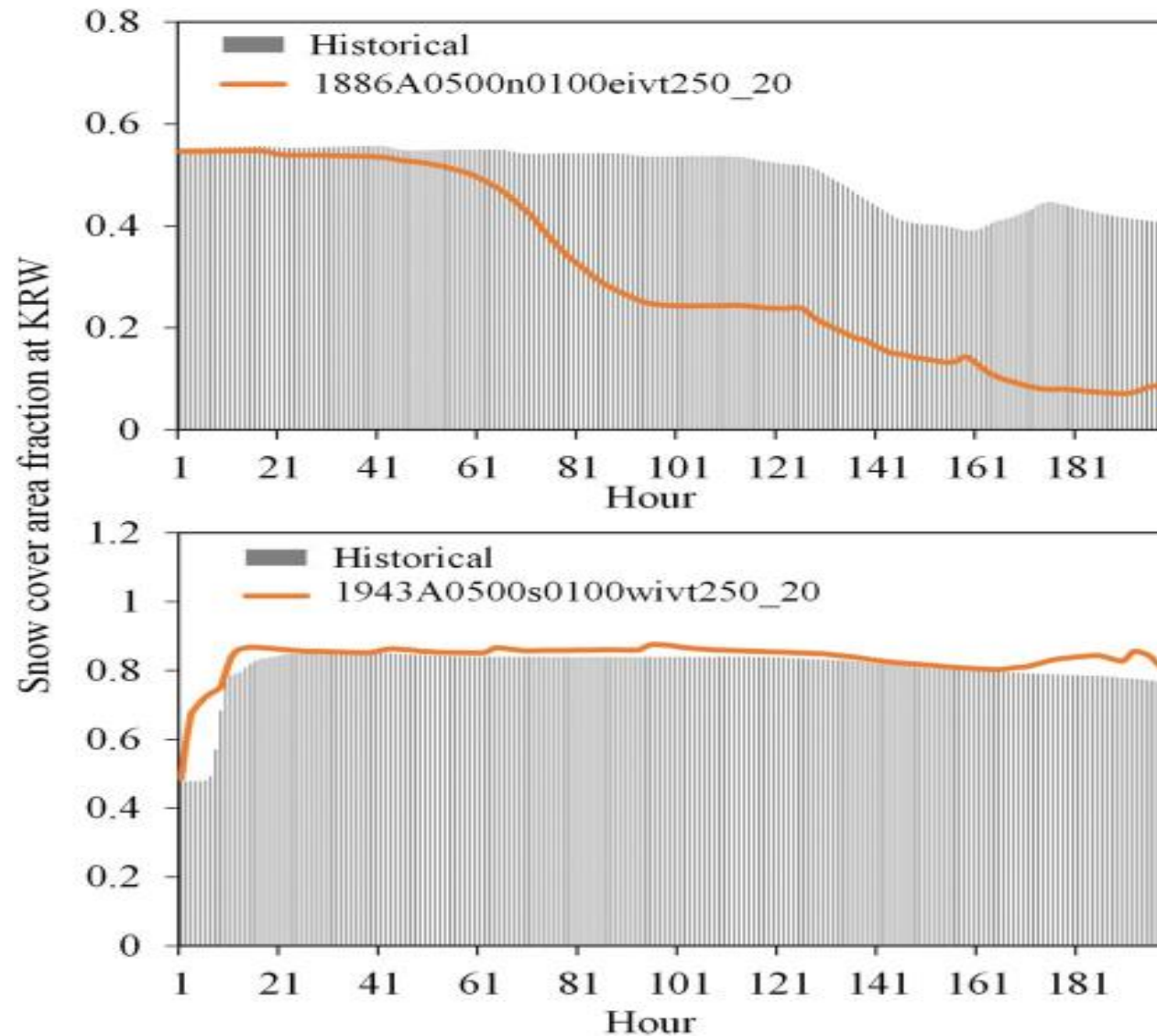
Validation comparisons of the daily mean discharge by WEHY simulations and the corresponding observations at each watershed during 10 years (1997–2006): (a) Cosumnes River watershed; (b) Upper Kings River watershed; (c) Mokelumne River watershed; (d) Stanislaus River watershed; (e) Tuolumne River watershed; (f) San Joaquin River watershed; (g) Merced River watershed

Ranked events over KRW (top 10)				
a. Ranked PMP events over KRW (top 10)				
Kings River Watershed (KRW)				
Event ID	Maximized 72-h precipitation (mm)	Rank	Historical 72-h precipitation (mm)	
1943A0500s0100wivt250_20	794.26	1	225.72	
1943A0500s0100wivt250_10	745.83	2	225.72	
1997A0500s0100wivt250_20	723.37	3	209.51	
1886A0500n0100eivt250_20	719.59	4	335.88	
1963B0200s0000eivt250_20	640.22	5	551.2	
1965A0500s0100eivt250_20	626.03	6	300.17	
1965A0500s0100wivt250_20	588.67	7	335.88	
1963B0100n0100e	570.94	8	551.2	
1963B0200n0100eivt250_12	542.89	9	551.2	
1885A0200s0100eivt250_20	516.06	10	121.35	
b. Ranked stream flow events with input from PMP events over KRW (top 10)				
Kings River Watershed (KRW)				
Event ID	Flow volume rank	Event flow peak (cm)	Historical flow peak (cm)	Event volume (m ³ x 10 ⁸)
1886A0500n0100eivt250_20	1	7035.7	2005.1	12.02
1943A0500s0100wivt250_20	2	4515.5	2058.2	4.96
1963B0200n0100eivt250_12	3	3176.8	2767.4	4.44
1943A0500s0100wivt250_100	4	3356.3	2058.2	4.4
1965A0500s0100eivt250_20	5	2836.8	1135.8	4.25
1963B0100n0100e	6	3038.6	2767.4	4.21
1963B0200s0000eivt250_20	7	2955.2	2767.4	4.16
1885A0200s0100eivt250_20	8	2505.5	583.43	3.8
1965A0500s0100wivt250_20	9	2461.9	1135.8	3.7
1995A0000n0100e	10	2256.2	1378.3	2.83

Ranked PMP and PMF events (top 10) at Upper Kings River Watershed (KRW)



Comparison of KRW basin-averaged temperature under historical and maximized precipitation conditions for the 1943 and 1886 events



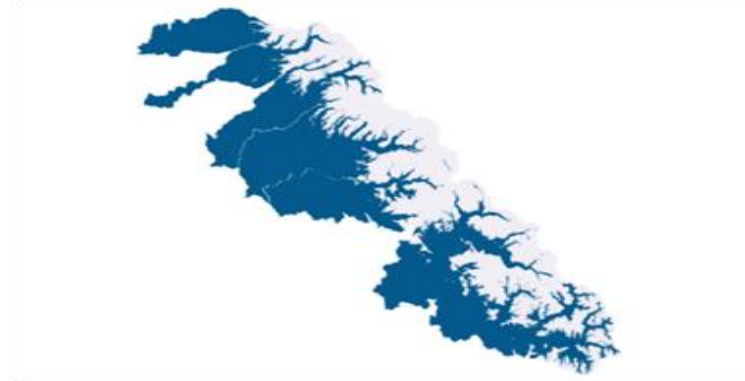
Comparison of KRW basin-averaged fractional snow cover for the historical and maximized precipitation conditions for the 1943 and 1886 events

1886

cP



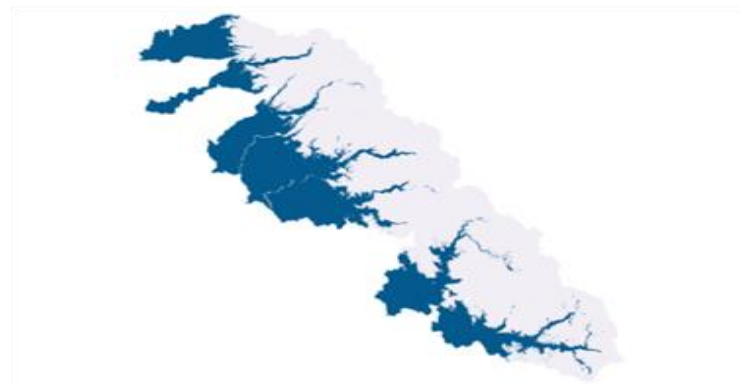
cPT



cT



Historical



Comparison of snow cover between the historical conditions and three different precipitation-temperature conditions during the 1886 event (ATMvar1886AcP, ATMvar1886AcPT, ATMvar1886AcT)

The maximization of extreme flood over the seven Southern California watersheds showed:

- 1) The flood event due to the maximum precipitation event does not necessarily result in the maximum flood;
- 2) The optimum combination of precipitation and temperature leads to the maximum flood event in snow-covered watersheds.

Physics-based numerical atmospheric-hydrologic modeling of the precipitation fields and floods as clusters of events has been addressed only recently (Hiraga et al. 2021, 2022; Kavvas et al. 2021, 2023). This topic still needs substantial new research.

Tropical Cyclones/Typhoons

Tropical Cyclones (TCs) are intense atmospheric vortices that form over the warm tropical oceans” (Chan and Kepert (2010)).

Approximately 80 TCs form worldwide every year (De et al., 2004).

Their life duration is very variable as TCs can last from 1 day to several weeks.

Even if TCs have usually horizontal extents of several hundreds of kilometers, the strongest winds, precipitation, and deep convection are located in a region of about 100 km in radius. As a consequence, TCs can be considered as mesoscale systems (Holton and Hakim, 2013).

More precisely, a calm eye with a diameter between 20 and 100 km and pressure deficit up to 10% of the ambient atmosphere is surrounded by a slantwise ring of deep convective clouds that extends through the whole troposphere. This ring is called the “eyewall”.

The primary circulation of a TC consists of the cyclonic flow around the storm center while the weaker secondary circulation consists of “inflow concentrated in the boundary layer, upflow in the eyewall and spiral rainbands, and outflow in a thin layer beneath the tropopause” (Chan and Kepert, 2010; Holton and Hakim, 2013). The secondary circulation is the energy source of the TC, and its working may be idealized as a Carnot machine (Cram et al., 2007; Emanuel, 1991) as illustrated in the following figure.

THREE POWERFUL HURRICANES, HURRICANE FRANCES,
HURRICANE IVAN AND HURRICANE JEANNE HIT EASTERN USA
WITHIN A SPAN 3.5 WEEKS DURING SEPTEMBER 2004

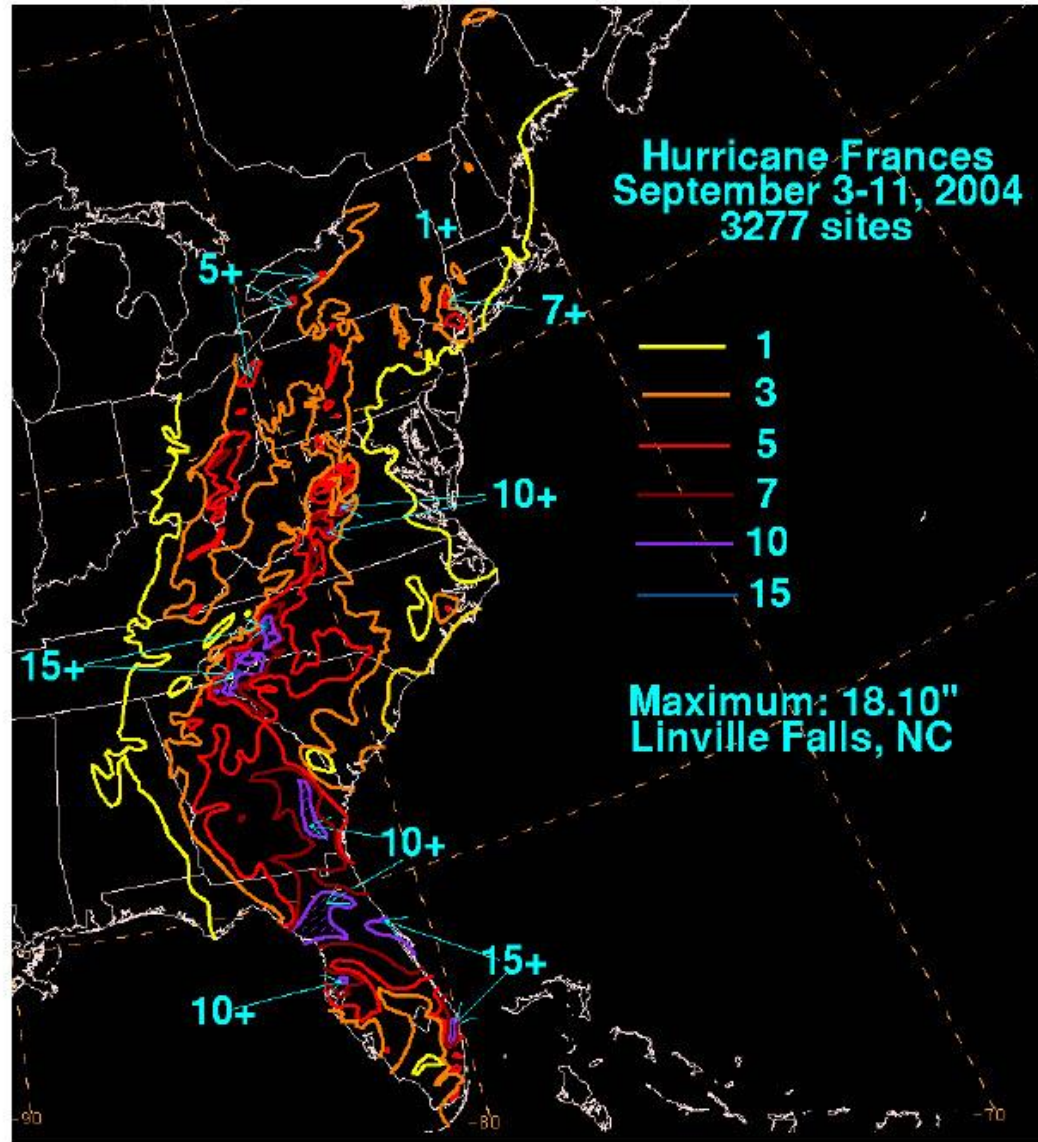
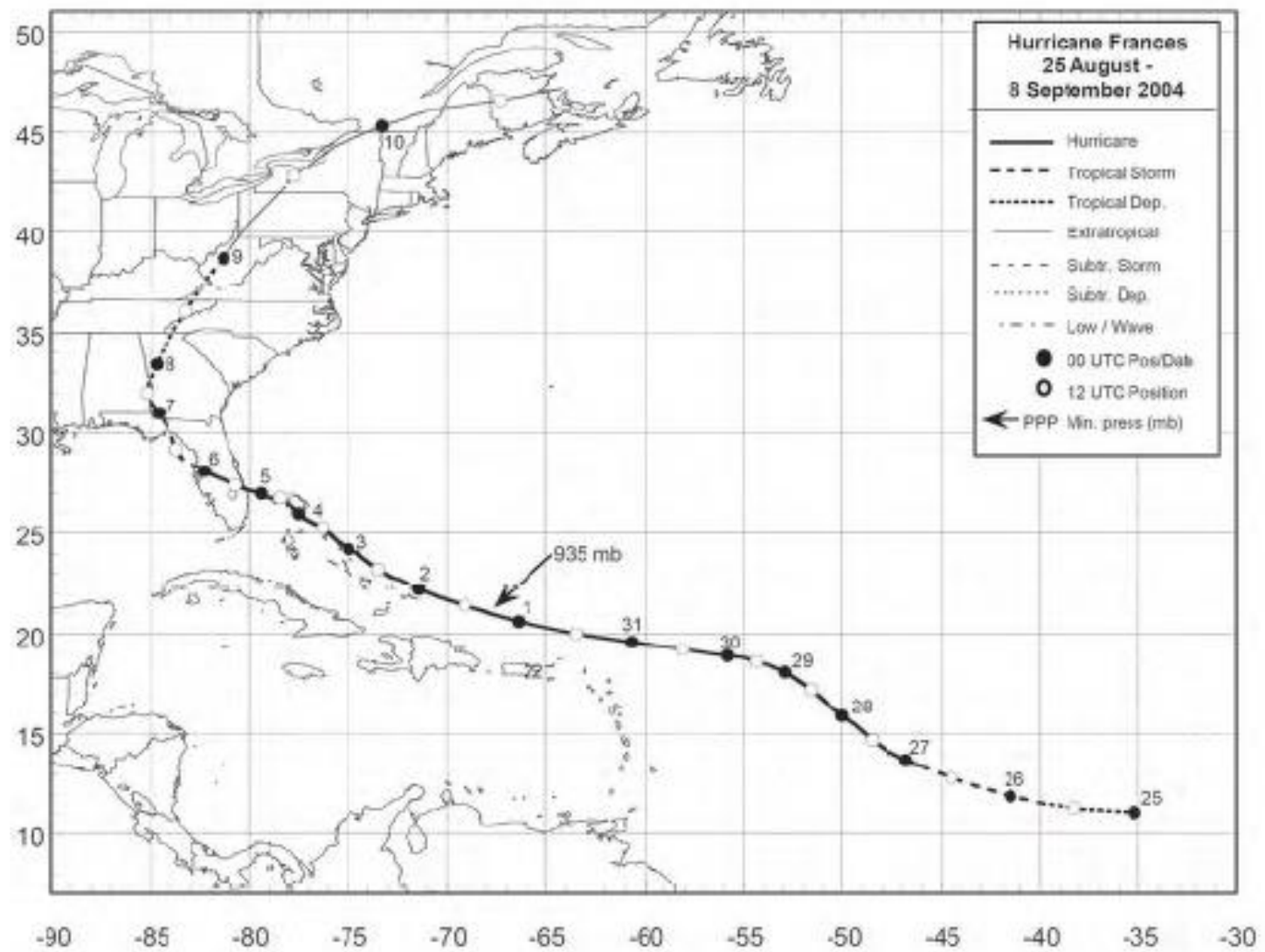


Figure 4. Storm-total rainfalls for Hurricane Frances, 25 August – 8 September 2004. Figure courtesy of David Roth of the Hydrometeorological Prediction Center.



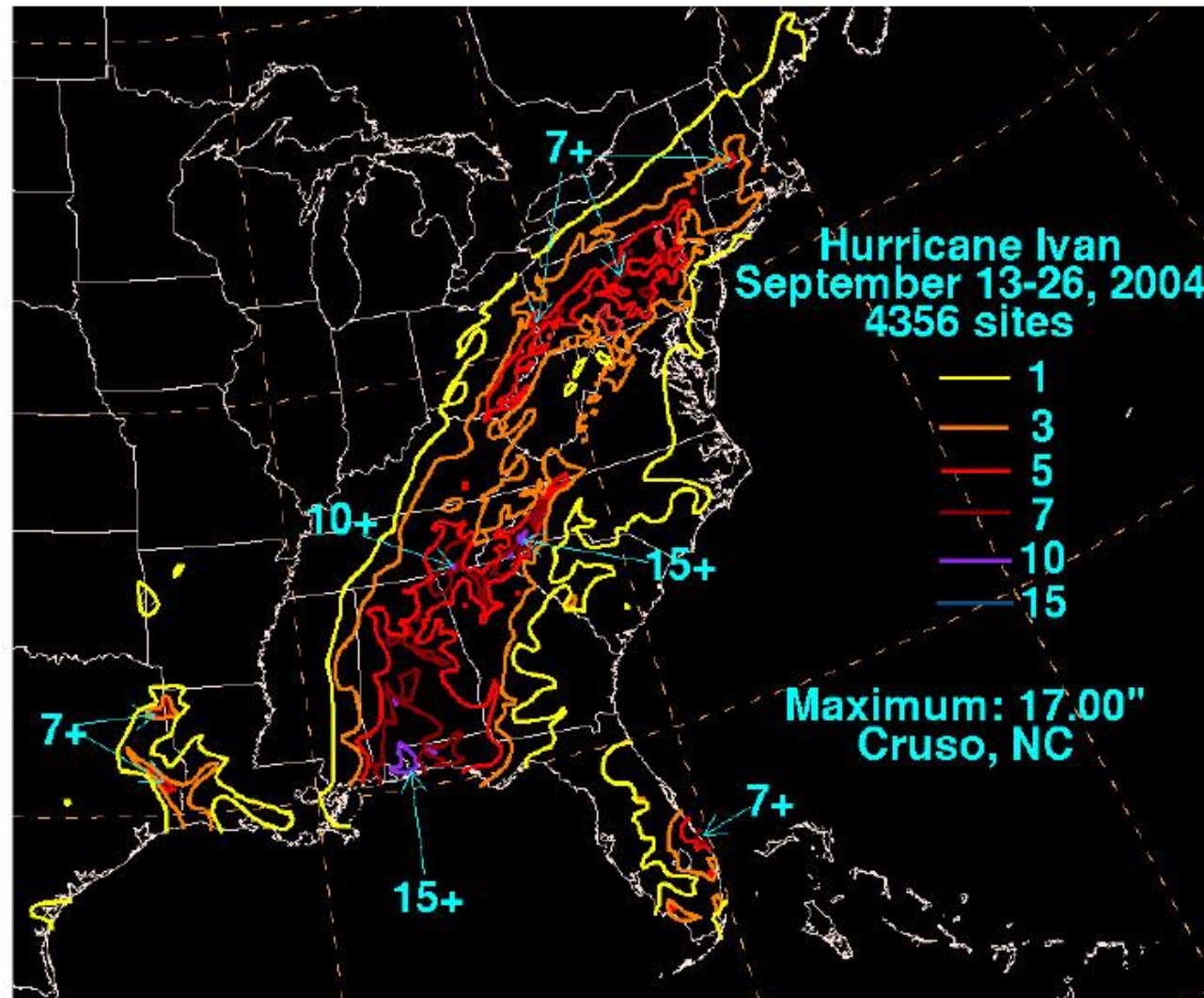
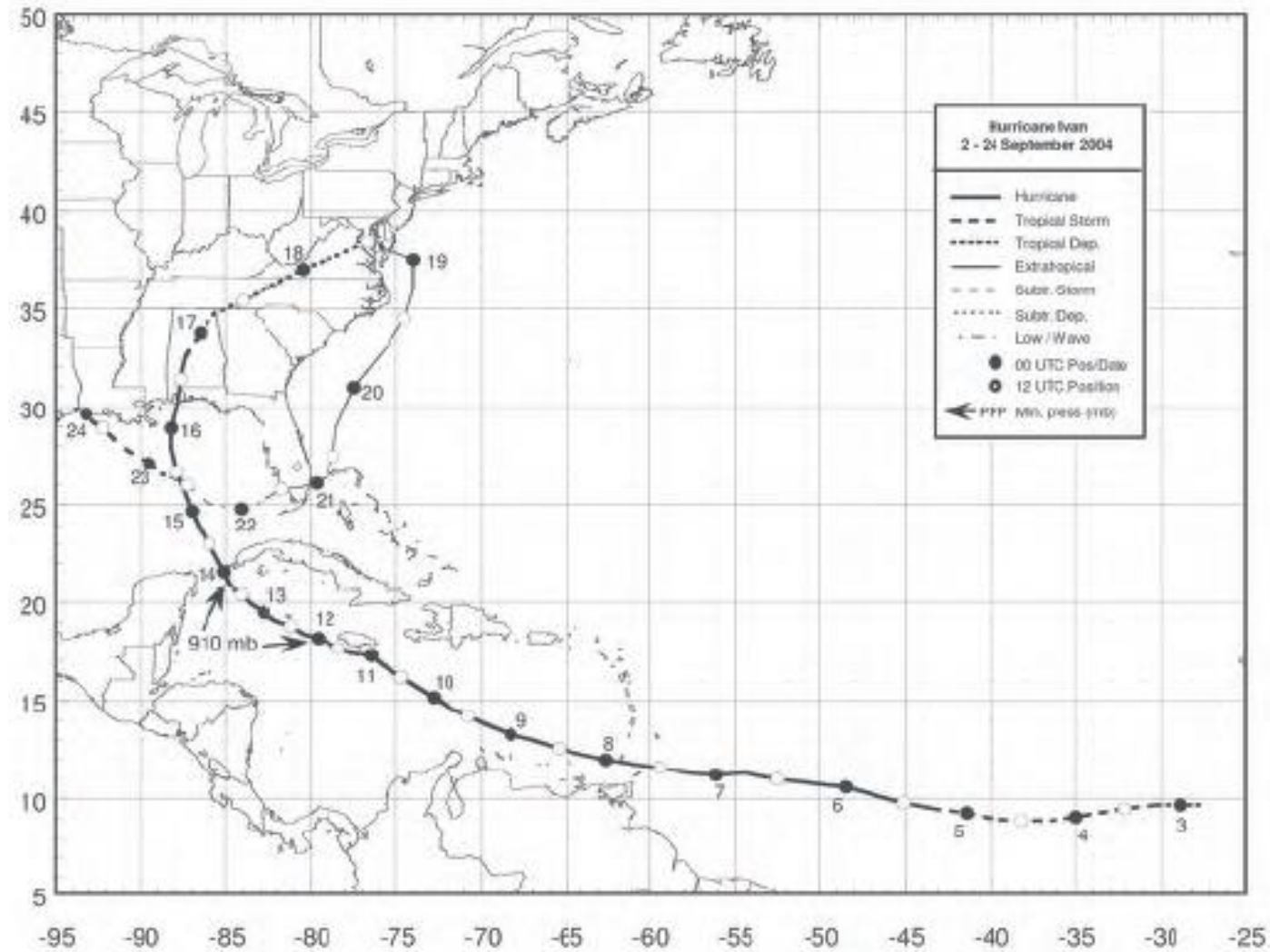
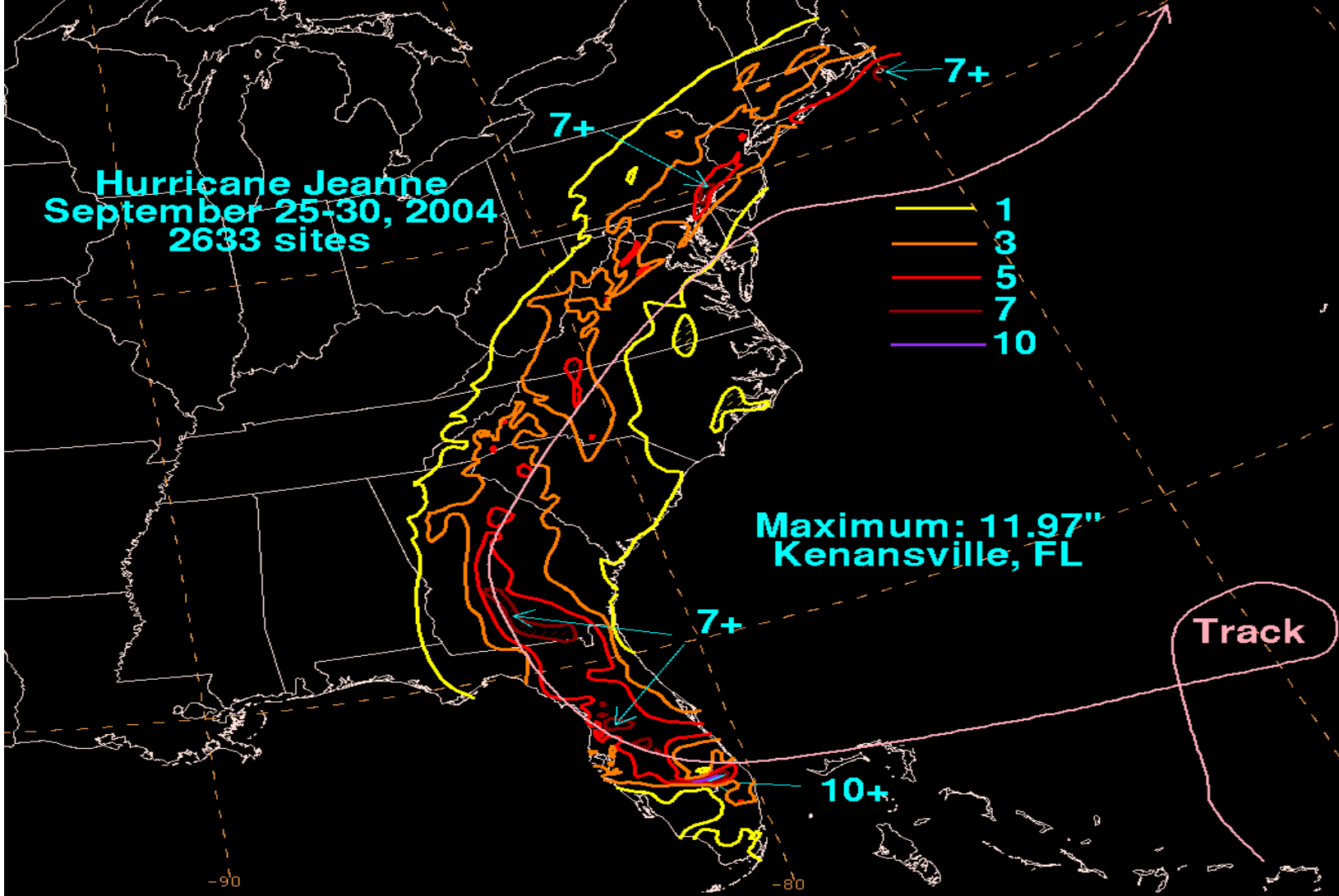


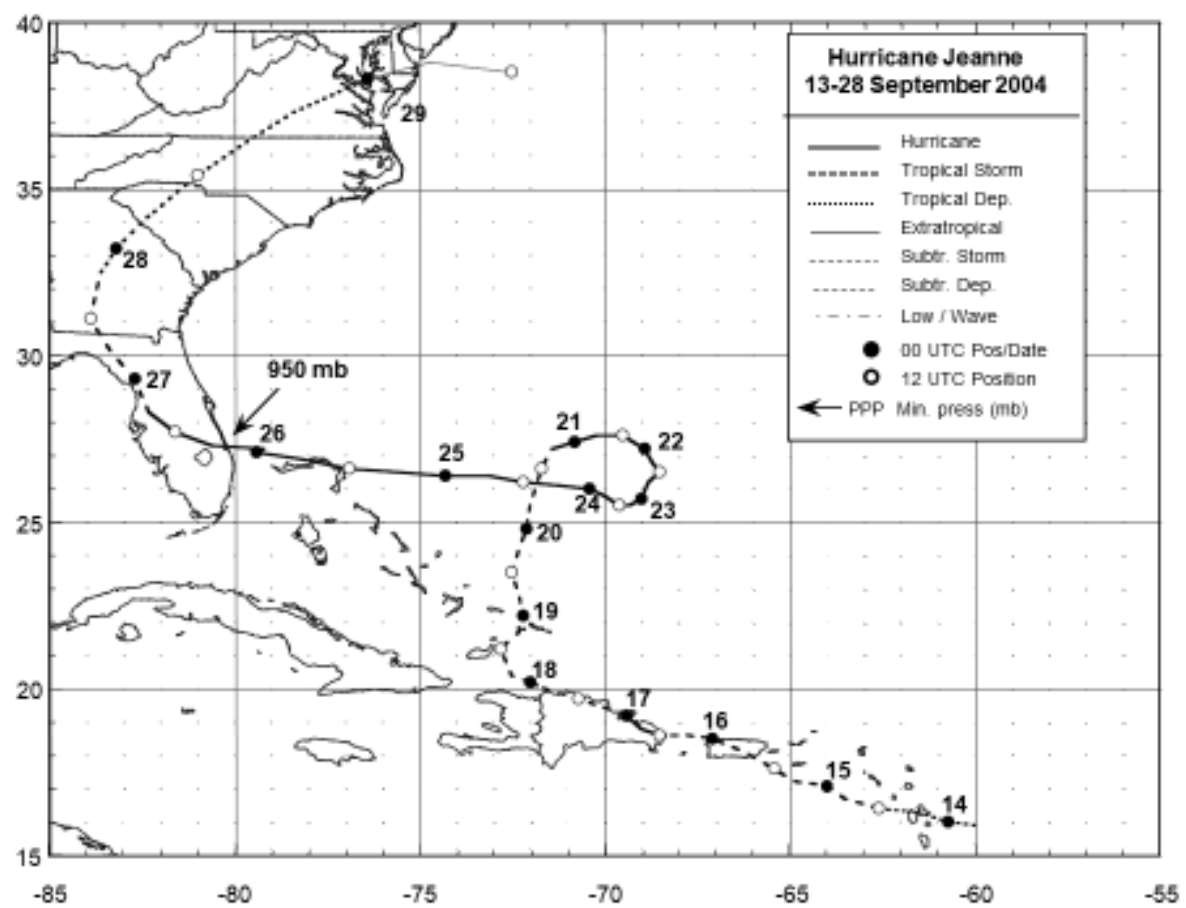
Figure 6. United States rainfall totals for Hurricane Ivan (image courtesy of NOAA Hydrometeorological Prediction Center).



Best track positions for the eye of Hurricane Ivan for September 3–24, 2004 (reproduced from Stewart, 2005). (Tropical Dep., Tropical Depression; Subtr. Storm, Subtropical Storm; Subtr. Dep., Subtropical depression; UTC, Universal Coordinated Time; mb, millibars).

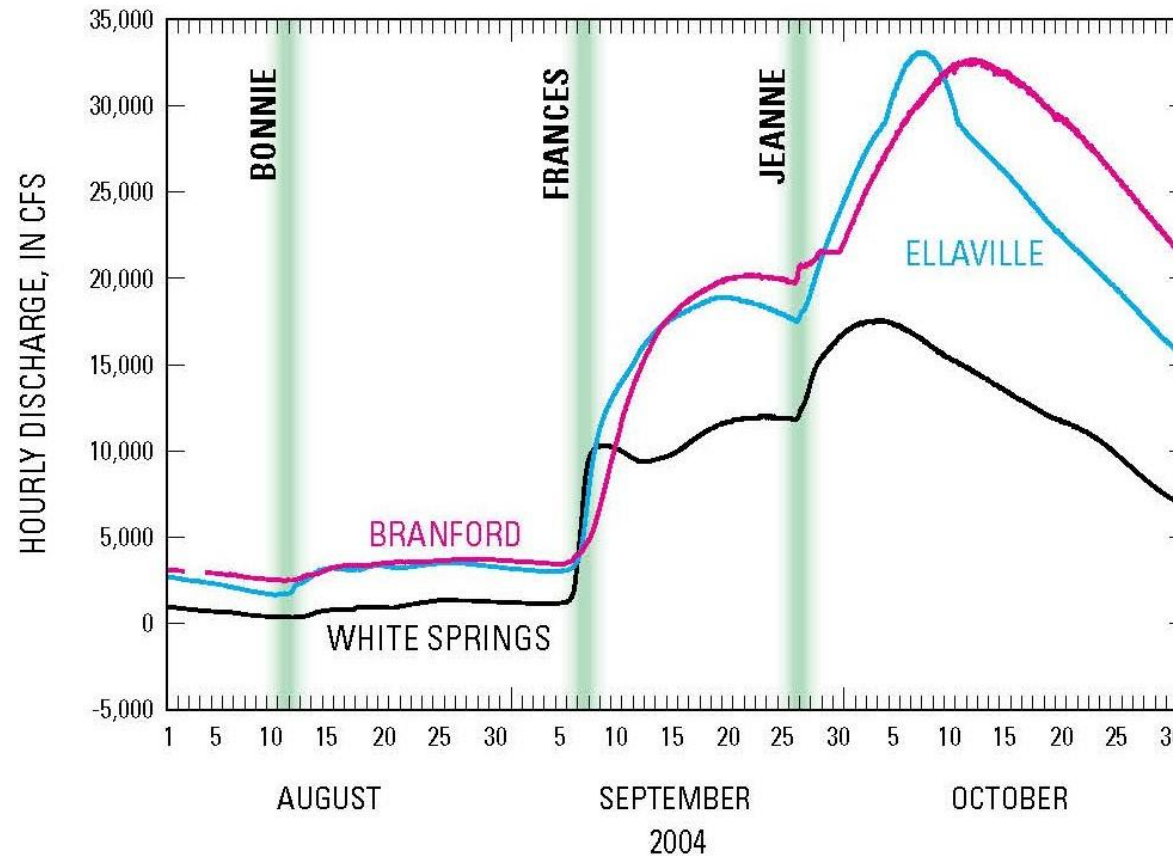


Storm total rainfall depth map (inches) of Hurricane Jeanne



Best track positions for Hurricane Jeanne, 13-28 September 2004.

Figure 16. Discharge hydrograph of the Suwannee River at White Springs, Fla.; Suwannee River at Ellaville, Fla.; and Suwannee River at Branford, Fla., showing increased discharge due to rainfall from Tropical Storm Bonnie, and Hurricanes Frances and Jeanne.



From “Hydrologic Effects of the 2004 Hurricane Season in NW Florida”, by R.J. Verdi, USGS Open-File Rept. 2005-1277

Hurricane Ivan

Hurricane Ivan developed over the tropical Atlantic Ocean, and on September 16. Ivan center came ashore as a category 3 hurricane just west of Gulf Shores, Alabama. Portions of the Interstate 10 bridge system across Pensacola, Florida were severely damaged due to the severe wave action on top of the 10-15 foot storm surge. Storm surge occurred all the way to Tampa Bay, Florida about 500 miles from Ivan's point of landfall.

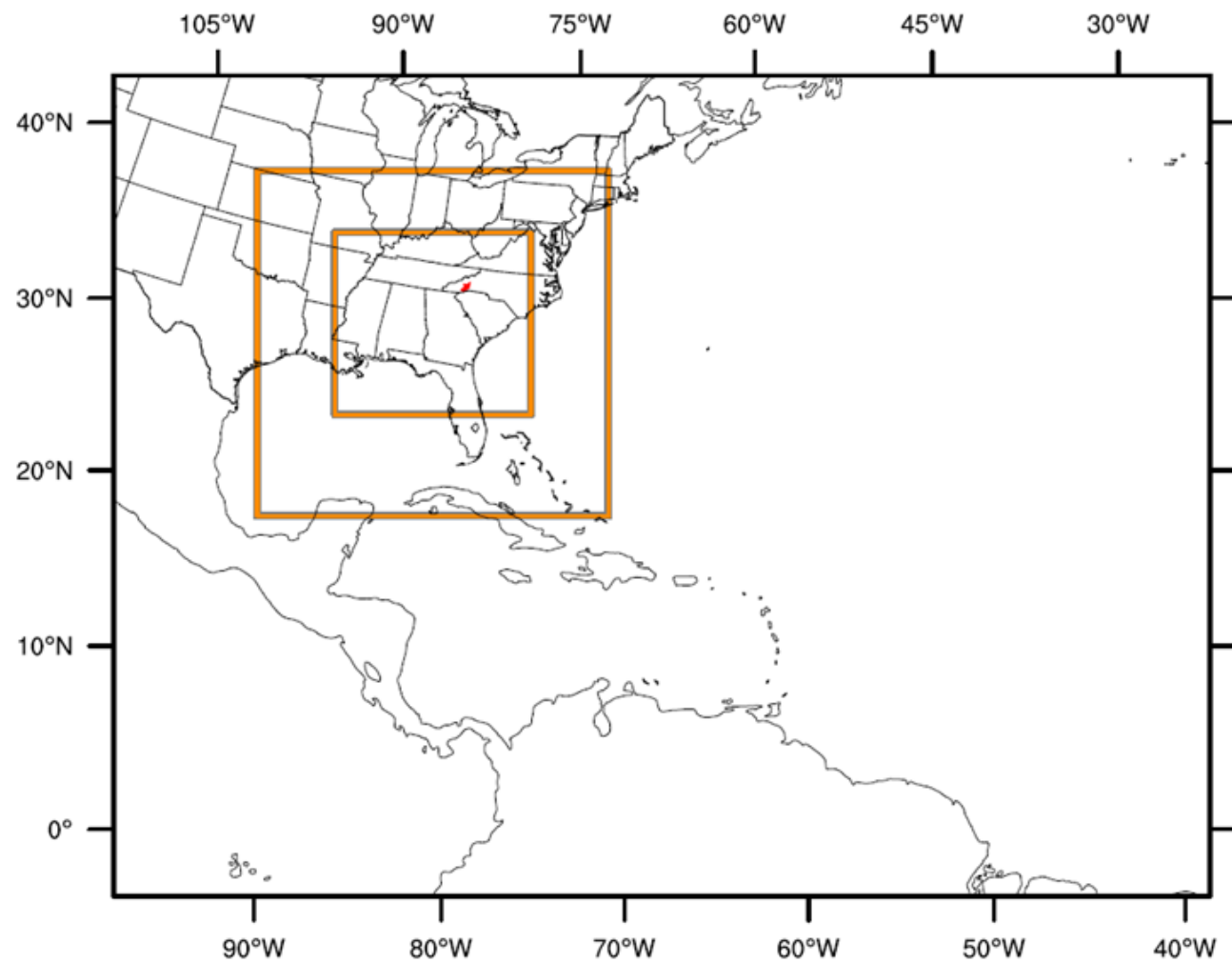
On September 16, 2004, Hurricane Ivan made landfall on the Gulf Coast at the Alabama–Florida border as a category 3 hurricane. It then moved northeast into Alabama. As Hurricane Ivan moved northeast on the evening of September 16, winds decreased and it was classified as a tropical storm over central Alabama.

As winds continued to decrease in the early morning of September 17, Ivan was classified as a tropical depression over northeast Alabama.

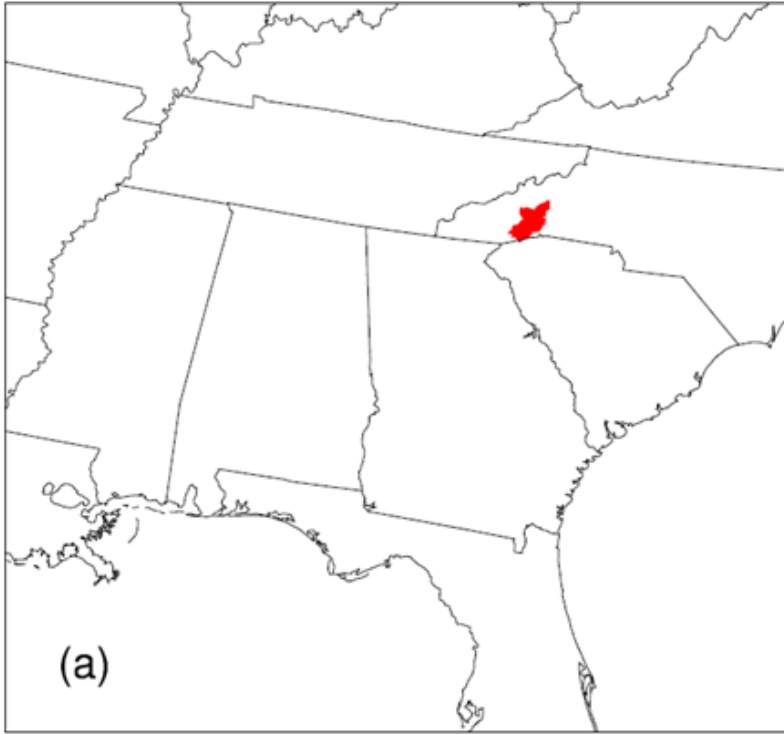
Ivan continued to move northeast across Tennessee and Virginia before it became extratropical over the Delmarva Peninsula on the afternoon of September 18.

Floods with recurrence intervals of 500 years or greater occurred at seven USGS stream gages throughout eastern Ohio during the Period of Hurricanes Frances and Ivan during August 28–September 27.

Fortunately, Hurricane Jeanne that followed Hurricane Frances and Hurricane Ivan, did not develop into a severe storm over most of Eastern USA, sparing the considerable destruction it could produce.



Nested domains used for the simulations of Hurricane Ivan. The small red area in western North Carolina is the target watershed



Target area used for the precipitation maximization by TC shifting. (a) The target area is shown in red within the model's inner domain. (b) The target area corresponds to the drainage basin of the city of Asheville, N.C.

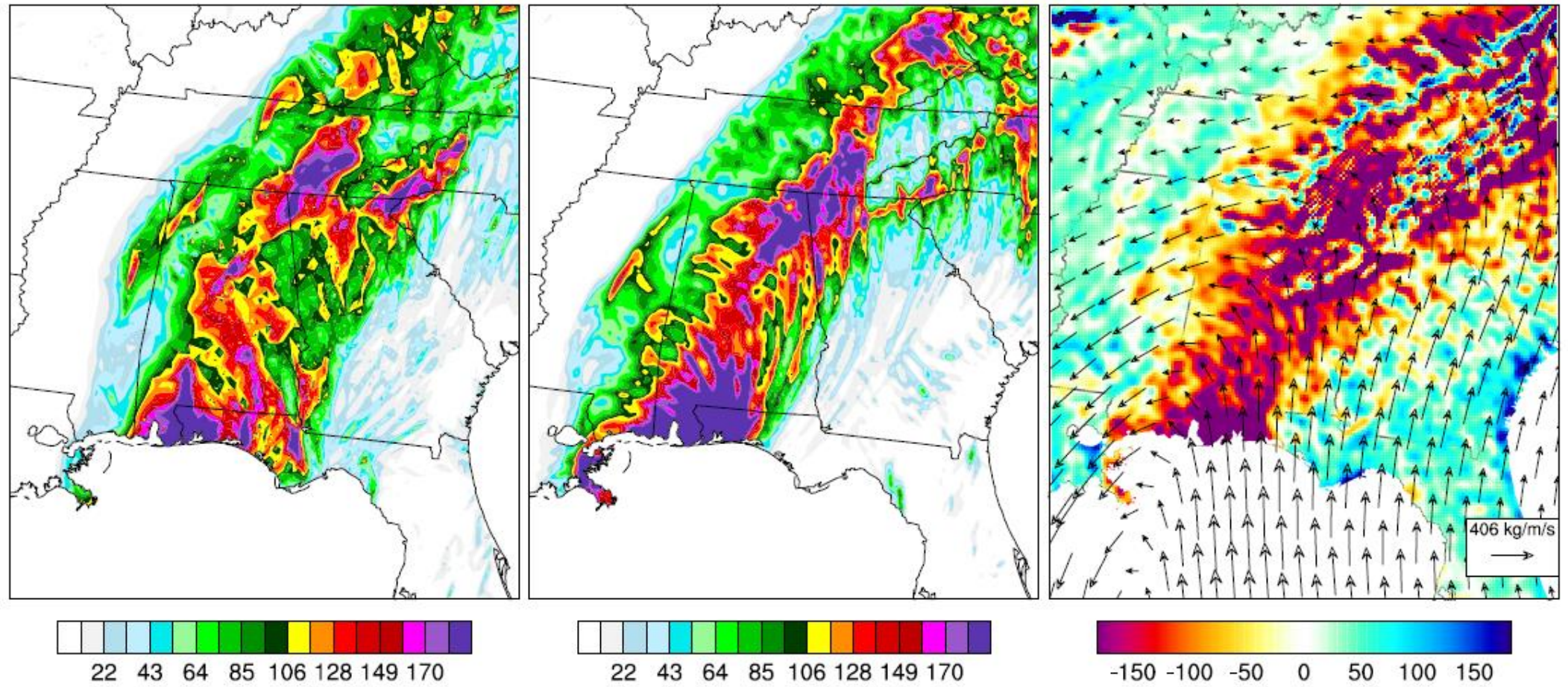
Numerical Simulation of Hurricane Ivan:

Two-way nesting was used for the simulations, meaning that the different domains (outer, intermediate and inner) are run simultaneously and communicate with each other. The top of the model was taken at 50 mbar, with a total of 38 vertical layers, and a time step of 3 minutes was used.

A simple 1-dimensional ocean mixed layer model was used following [Pollard et al. \(1972\)](#). The parameterization schemes used for the simulations of Hurricane Ivan are given in the below table. This combination of the parameterization schemes comes from the configuration of the WRF model for the reconstruction of Hurricane Ivan. Cumulus parameterization was used only in the outer and intermediate domains. The simulation start date is 09/06/2004 00:00 UTC. At that time, Hurricane Ivan was located off the coast of French Guyana and Suriname.

Parameterization schemes used for the simulations of Hurricane Ivan

Microphysics	WRF Double Moment 6-class (WDM6)
Cumulus Parameterization (domains 1 and 2 only)	New Simplified Arakawa-Schubert (SAS)
Planetary Boundary Layer	Mellor-Yamada-Janvic (MYJ)
Longwave Radiation	Rapid Radiative Transfer Model (RRTM)
Shortwave Radiation	Dudhia
Land Surface	Unified Noah Land Surface Model
Surface Layer	Eta Similarity Scheme



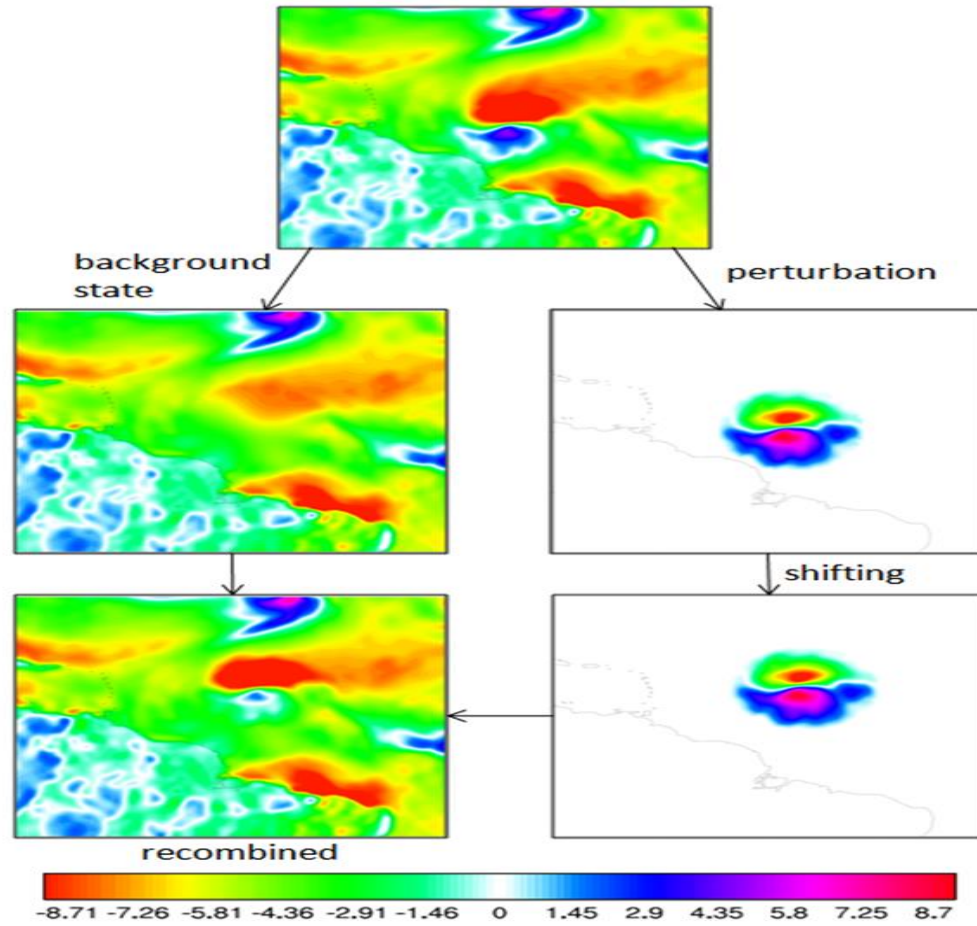
(a) Hurricane Ivan observed accumulated precipitation field in the inner-domain (from 09/14 00:00 UTC to 09/19 00:00 UTC). (b) Inner-domain WRF-simulated accumulated precipitation field (from 09/14 00:00 UTC to 09/19 00:00 UTC). (c) Arrow field: time-averaged (from 09/14 00:00 UTC to 09/19 00:00 UTC) integrated vapor transport ($\text{kg m}^{-1} \text{s}^{-1}$). Color plot: divergence of the time-averaged integrated vapor transport field (mm).

Description of the Tropical Cyclone/Hurricane/Typhoon Storm Transposition (Shifting) method

Initial and boundary conditions used for dynamical downscaling with a Regional Atmospheric Model (RAM) are usually obtained from the outputs of a general circulation model (GCM) or Reanalysis Data. This section presents a method to shift the location of a TC in the initial conditions. The objective of this transposition is to modify the track of the storm so that its precipitation field moves over a specified target area.

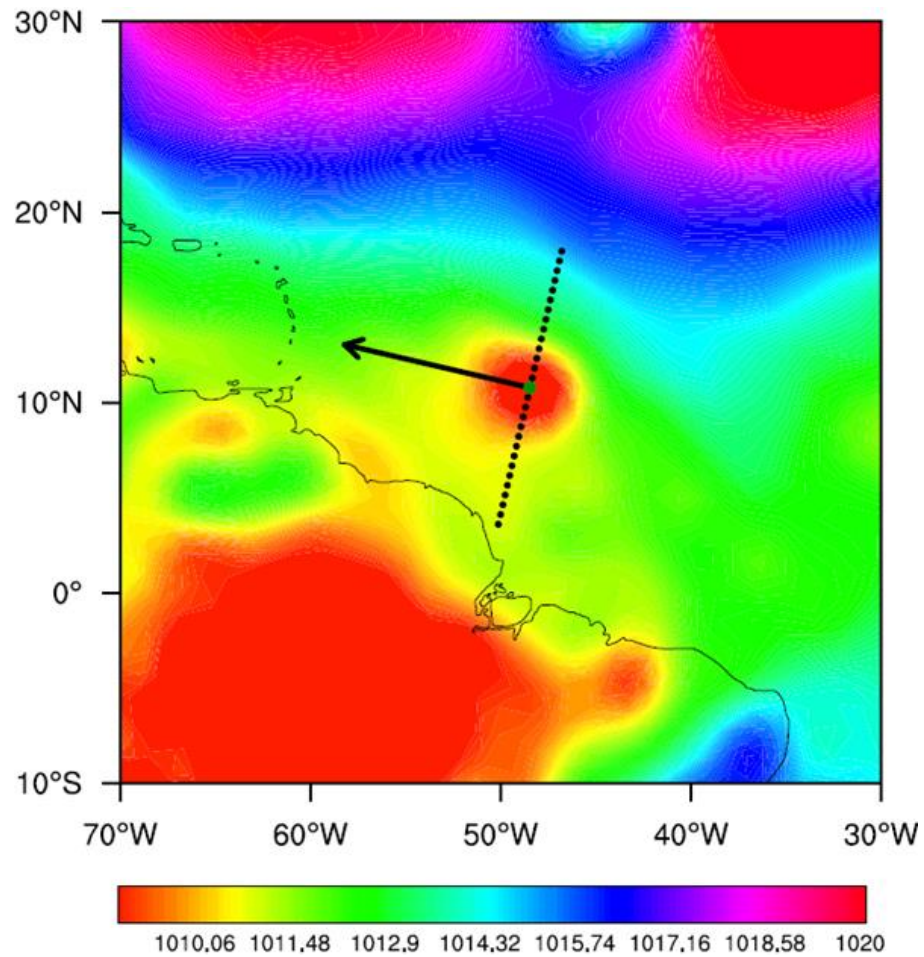
The transposition of the TC in the initial conditions is performed by executing the following procedure:

1. Identify the location (x_c, y_c) of the center of low pressure;
2. Identify the radius R of the cyclone;
3. Remove the TC from the background atmospheric fields by cutting off the inside of the circle of center (x_c, y_c) and of radius R from the original atmospheric fields;
4. Interpolate the background fields to the inside of the circle;
5. Compute the perturbation fields by subtracting the background fields obtained in step 4 from the original fields. The perturbation fields are zero everywhere except inside the circle;
6. Shift the perturbation fields;
7. Add the shifted perturbation fields to the corresponding background fields obtained in step 4.

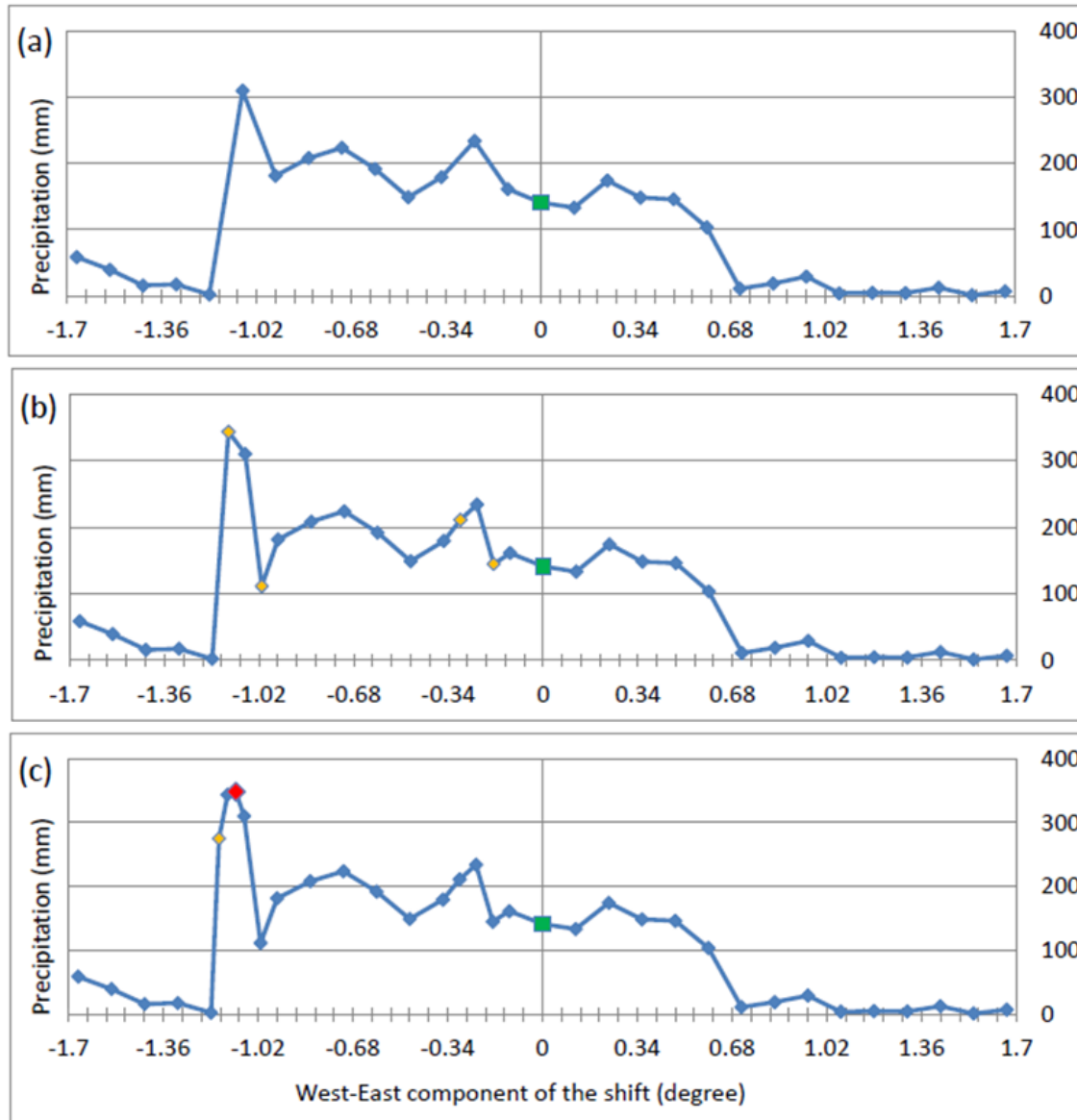


Application of the transposition (shifting) procedure to the initial surface zonal wind velocity ($\text{m}\cdot\text{s}^{-1}$) in Hurricane Ivan.

Hurricane Ivan was transposed in a direction orthogonal to its direction of propagation at the simulation start date (below figure). The transposition exercise was first performed for 29 amounts of shift (including zero shift), from 1.67 degree west and 7.18 degree south to 1.67 degree east and 7.18 degree north, which corresponds to the black dots in below figure. The WRF model was run for each of these amounts of shift, and the maximum 72-hour (3-day) accumulated precipitation over the target watershed, which corresponds to the 72-h time window that contains the largest basin average precipitation, was calculated for every simulation. Results for this first step are presented in the second figure below. Note that the shifting results are represented by plotting them only against the West-East component of the shift that occurs along the line of black dots shown in the below figure.



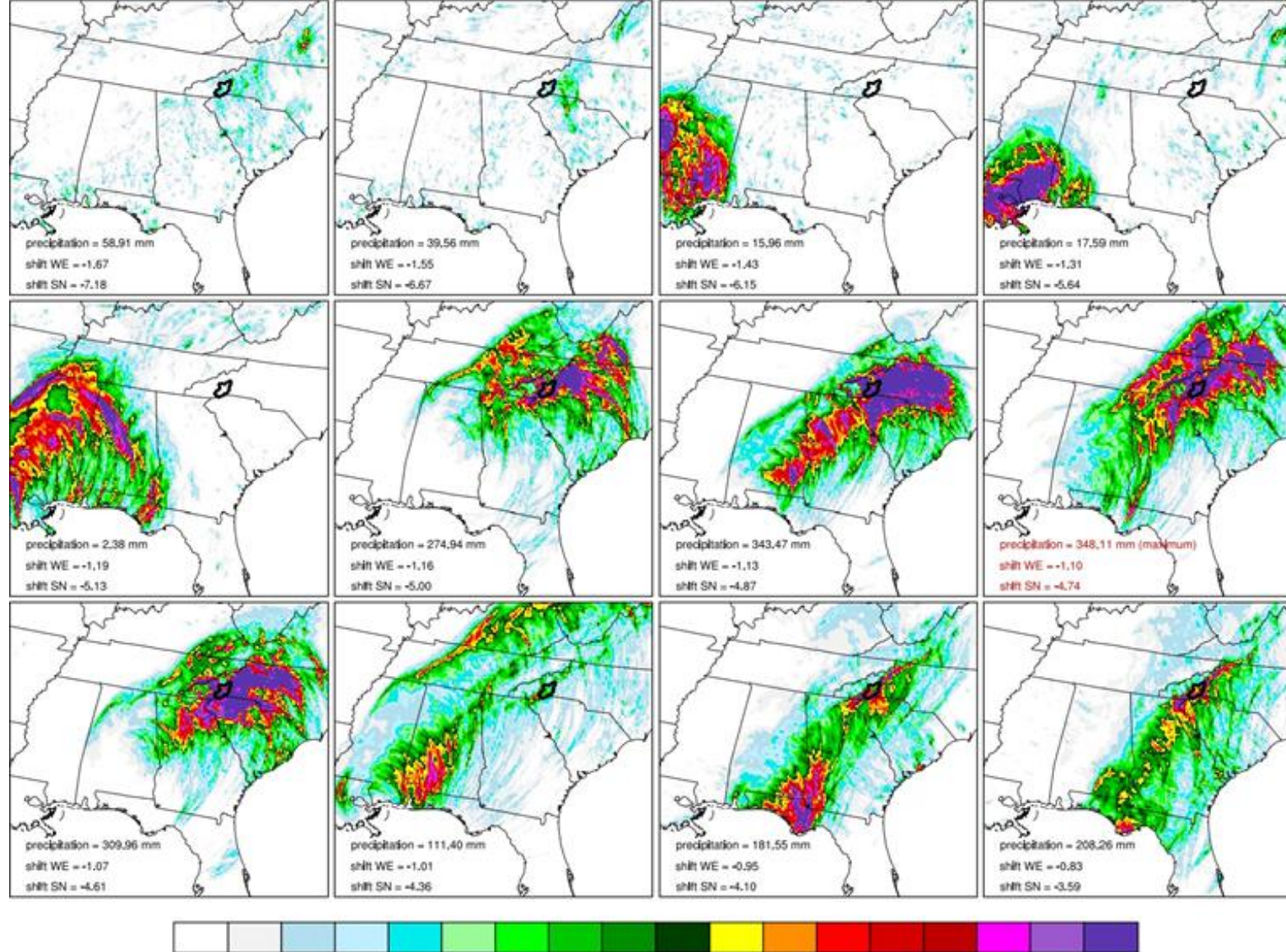
The color plot shows the mean sea level pressure field (mbar) on 09/06/2014 00:00 UTC (from CFSR) for zero shift. The green point gives the location of the center of low pressure in the original TC (zero shift). The black points give the location of the center of low pressure after shifting. The black arrow indicates the direction of propagation of Hurricane Ivan.



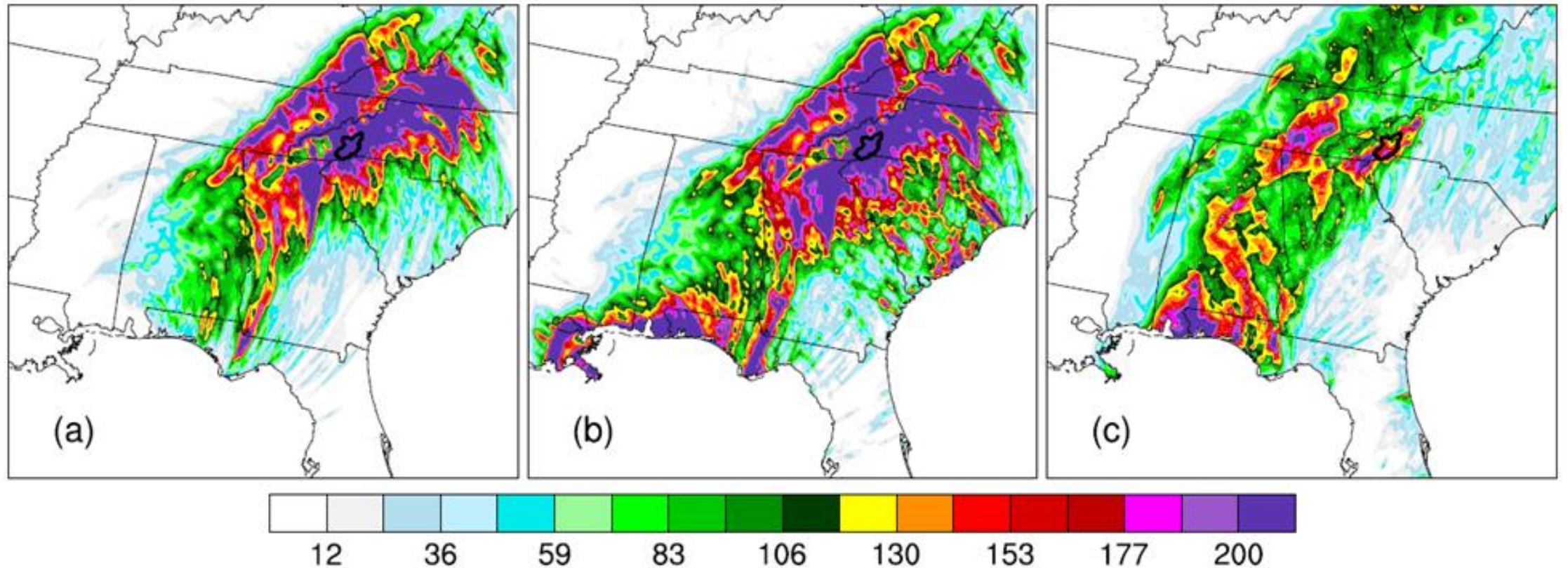
72-h basin average precipitation as a function of the West-East component of the shift. (a) Results for the 29 shifts in degrees first considered (above figure). (b) Results after the first refinement. (c) Results after the second refinement. The green square gives the 72-h basin average precipitation in the case of no shift. The yellow diamonds show the refinement performed around the local maxima. The red diamond in (c) indicates the maximum 72-h basin average precipitation.

Above figure shows that Hurricane Ivan responds nonlinearly to the transposition of its initial conditions. Indeed the location of the precipitation field does not change homogeneously as the amount of shift is increased from 1.67 degrees west and 7.18 degrees south to 1.67 degrees east and 7.18 degrees north. For example, the 72-h accumulated precipitation field corresponding to an amount of shift of 1.07 degrees west and 4.61 degrees south (third plot on Row 2 in above figure) is located east of the 72-h accumulated precipitation field corresponding to an amount of shift of 1.01 degrees west and 4.36 degrees south (fourth plot on Row 2 in above figure). This behavior explains the presence of multiple peaks in the graphs of the 72-h basin average precipitation as a function of the zonal component of the shift presented in the figure before the above figure.

Given 1) the strong nonlinearity involved in the dynamics of a TC, 2) the fact that we used no nudging and data assimilation, and 3) the early simulation start date (about ten days before the time of landfall), it is not expected that the numerical model manages to reproduce accurately the track of the TC, including the time and location of landfall. In order to place the simulated precipitation field in the right location, it is necessary to use a later simulation start date, as was done for the configuration of the WRF model for which the simulation start date was only two days before the time of landfall.



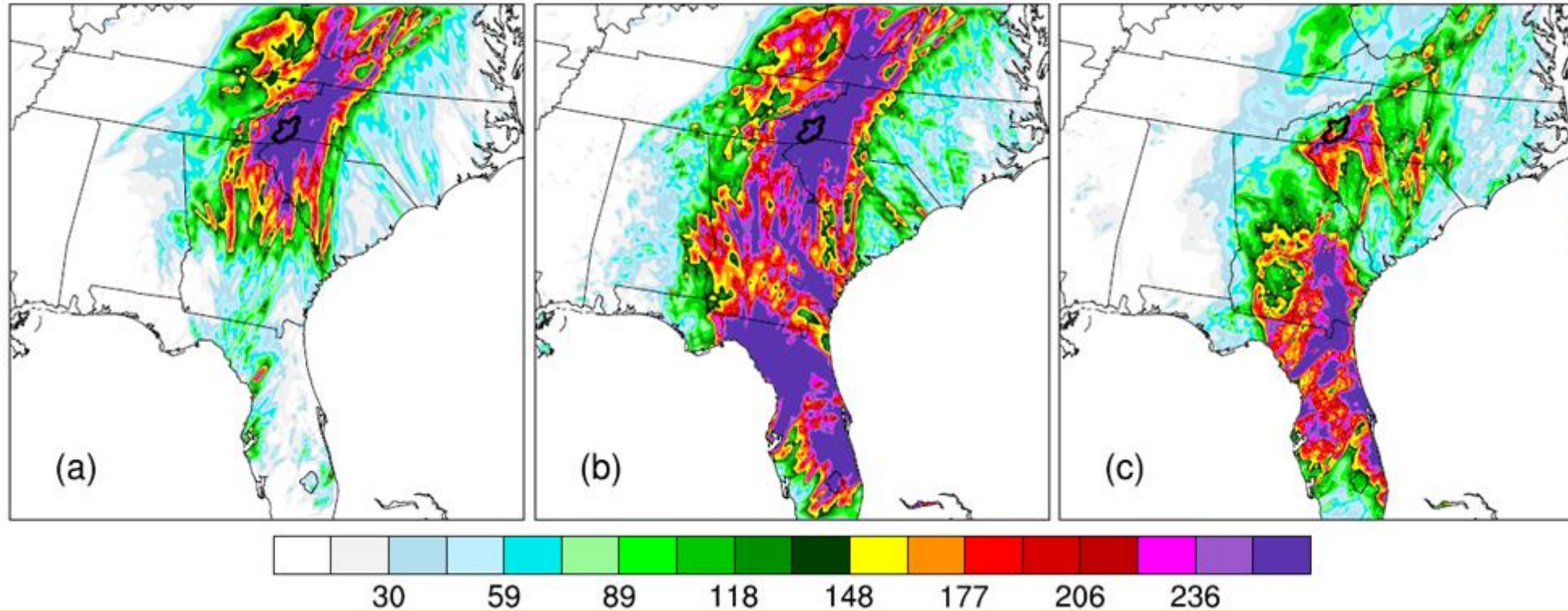
72-h accumulated precipitation field as a function of the amount of shift. The first plot (top-left) corresponds to the most westerly and southerly shift (1.67 degrees west and 7.18 degrees south) while the last plot (bottom-right) corresponds to the most easterly and northerly shift (1.67 degrees east and 7.18 degrees north). The maximum 72-h basin average precipitation is obtained for the 8th plot (fourth plot on Row 2).



(a) 72-h accumulated precipitation (mm) field (from 09/16 08:00 UTC until 09/19 08:00 UTC) for the simulation which maximized the 72-h basin average precipitation. (b) 7-day accumulated precipitation field (from 09/14 00:00 UTC until 09/21 00:00 UTC) for the simulation which maximized the 72-h basin average precipitation. (c) Observed 7-day accumulated precipitation field (from 09/14 00:00 UTC until 09/21 00:00 UTC).

It is observed that the maximized precipitation field is overall significantly more intense than the observed field, which shows that the physically based transposition method does not result in a simple transposition of the storm's precipitation field, as it is often assumed in the traditional PMP approaches. While the maximized 7-day precipitation over the Asheville watershed is around 200 mm, the observed 7-day precipitation due to Hurricane Ivan is in the 80 – 190 mm range. In about half of the watershed area the observed 7-day precipitation is less than 130 mm.

PRECIPITATION MAXIMIZATION OF HURRICANE FRANCES OVER EASTERN USA



(a) 72-h (from 09/06/2004 23:00 UTC until 09/09/2004 23:00 UTC) accumulated precipitation (mm) field in Hurricane Frances for the simulation which maximized the 72-h basin average precipitation. (b) 7-day (from 09/04/2004 00:00 UTC until 09/11/2004 00:00 UTC) accumulated precipitation field in Hurricane Frances for the simulation which maximized the 72-h basin average precipitation. (c) Observed 7-day (from 09/04/2004 00:00 UTC until 09/11/2004 00:00 UTC) accumulated precipitation field in Hurricane Frances.

While the maximized 7-day precipitation over Asheville watershed is around 260 mm, the observed 7-day precipitation over Asheville watershed due to Hurricane Frances is in the 74-192 mm range. Half of the watershed area during the observed Hurricane Frances receives less than 118 mm 7-day precipitation.

Hurricanes Frances (9/4 – 9/11/2004), Ivan (9/13 – 9/28/2004) and Jeanne (9/25 – 9/30/2004) were clustered in time within a 3-weeks period, following each other sequentially.

Such a historical occurrence of three hurricanes in a sequence within a time window of 3 weeks is not addressed in any of the conventional extreme precipitation estimation approaches, nor in the conventional extreme flood estimation approaches.

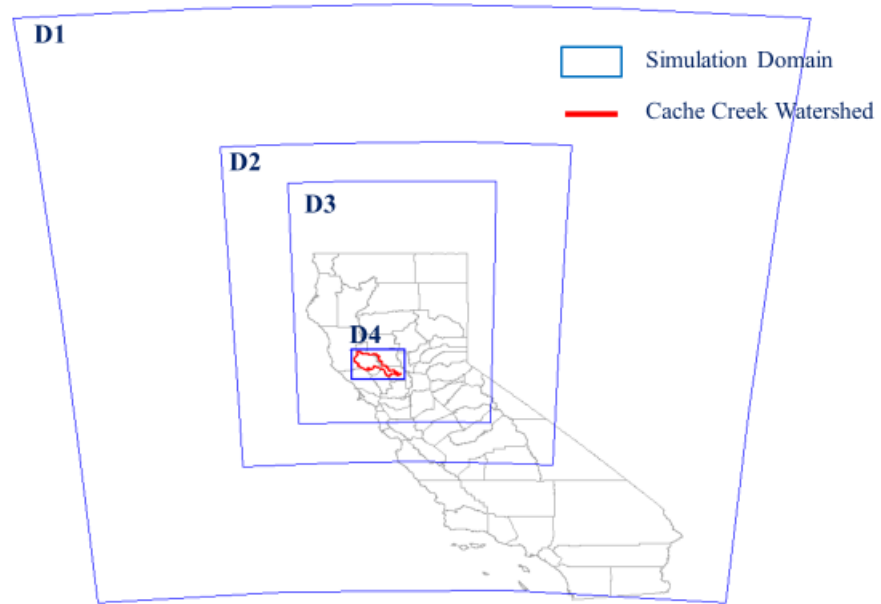
As may be seen from their maximized precipitation states over the Asheville watershed, if these hurricanes would hit the watershed in their maximized forms, they would produce tremendous flooding and resulting disaster.

The reported study was confined only to the maximization of precipitation fields. As such, the resulting Probable Maximum Flood could not be estimated.

Estimation of the Return Periods of Extreme Floods under Changing Climate

One approach to the estimation of extreme flood return periods under the evolving hydro-climate of the 21st century, is by means of the integrated atmospheric-hydrologic numerical model simulations of the extreme floods, based on an ensemble of GCM hydro-climate projections that will cover a range of possible emission scenarios (Kavvas et al. 2017; Trinh et al. 2016)

**Regional Hydro-Climate Model Simulation Domain
for Cache Creek Watershed**



Trinh et al. (2016)

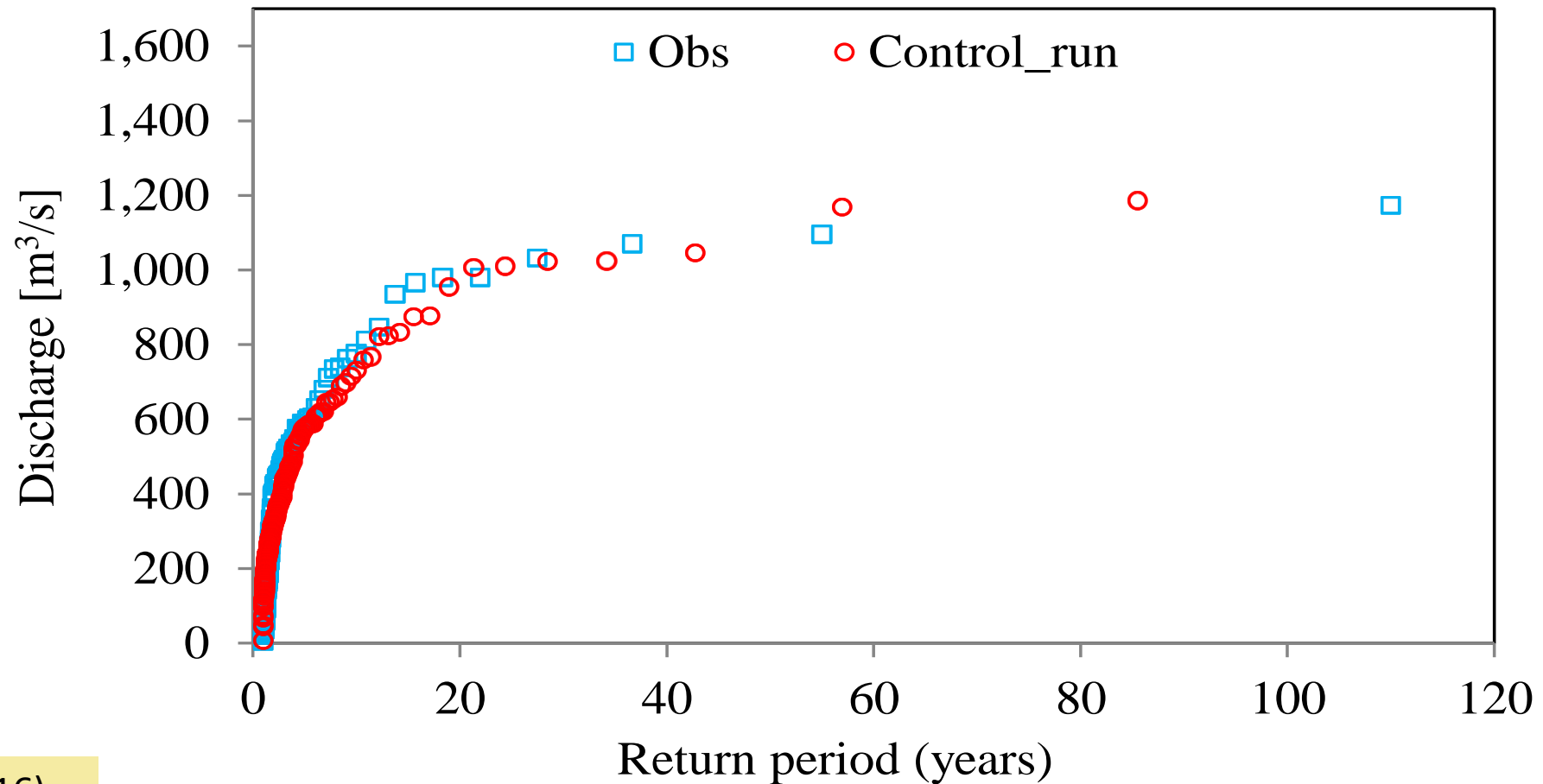
GCMs and Scenarios Used

	Models	Available realizations	GCM grid resolutions	Simulation period	Spatial Scale	Temporal scale
Historical Control Runs	ECHAM5	-	1.8°	1900-1999	9 km	1-hour
	CCSM3	-	1.4°	1900-1999	9 km	1-hour
21 st century projections	ECHAM5	9	1.8°	2010-2099	9 km	1-hour
	CCSM3	4	1.4°	2010-2099	9 km	1-hour

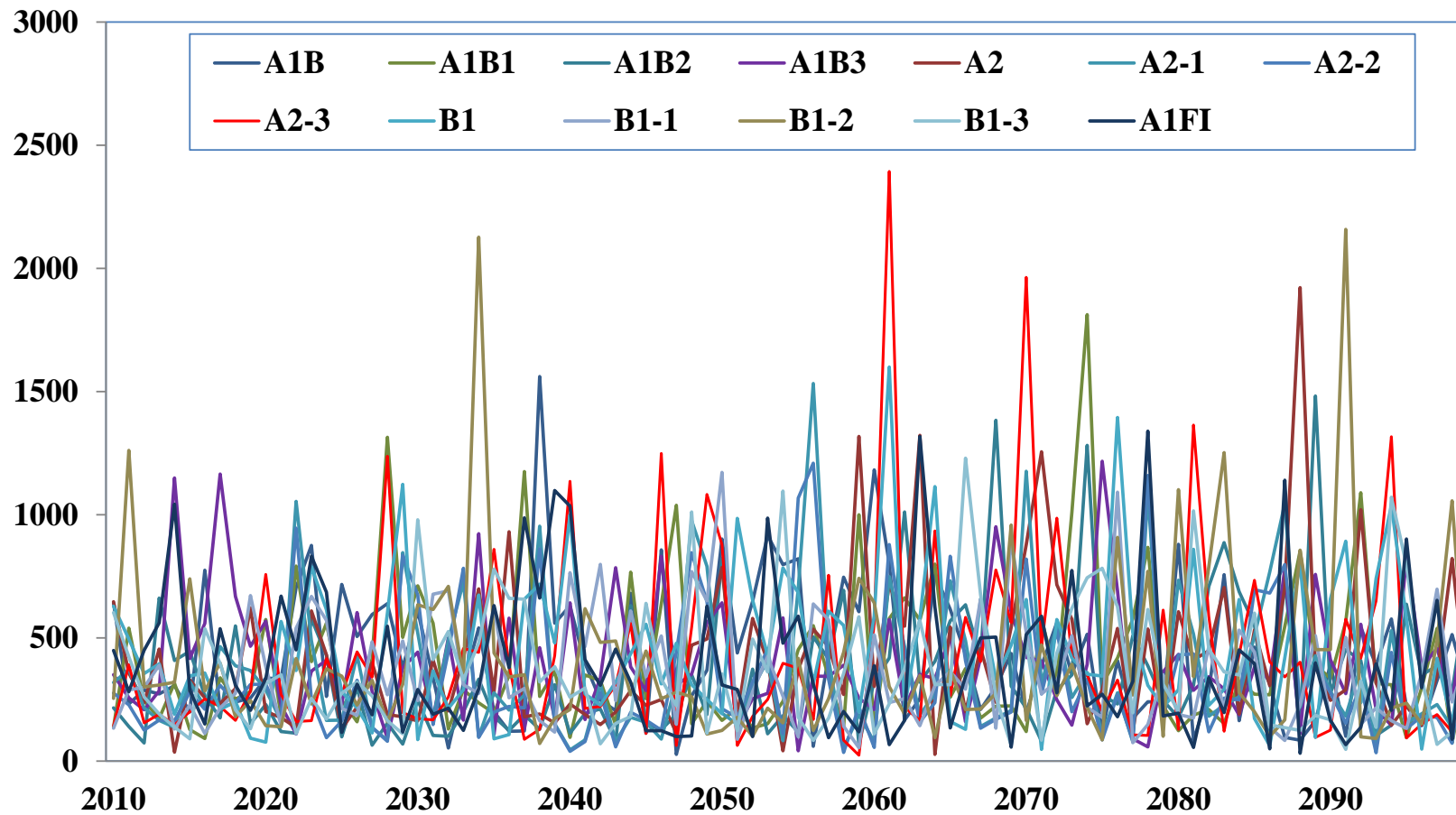
ECHAM5 (Scenarios): A1B1, A1B2, A1B3, A2-1, A2-2, A2-3, B1-1, B1-2, B1-3

CCSM3 (Scenarios): A1B, B1, A2, A1FI

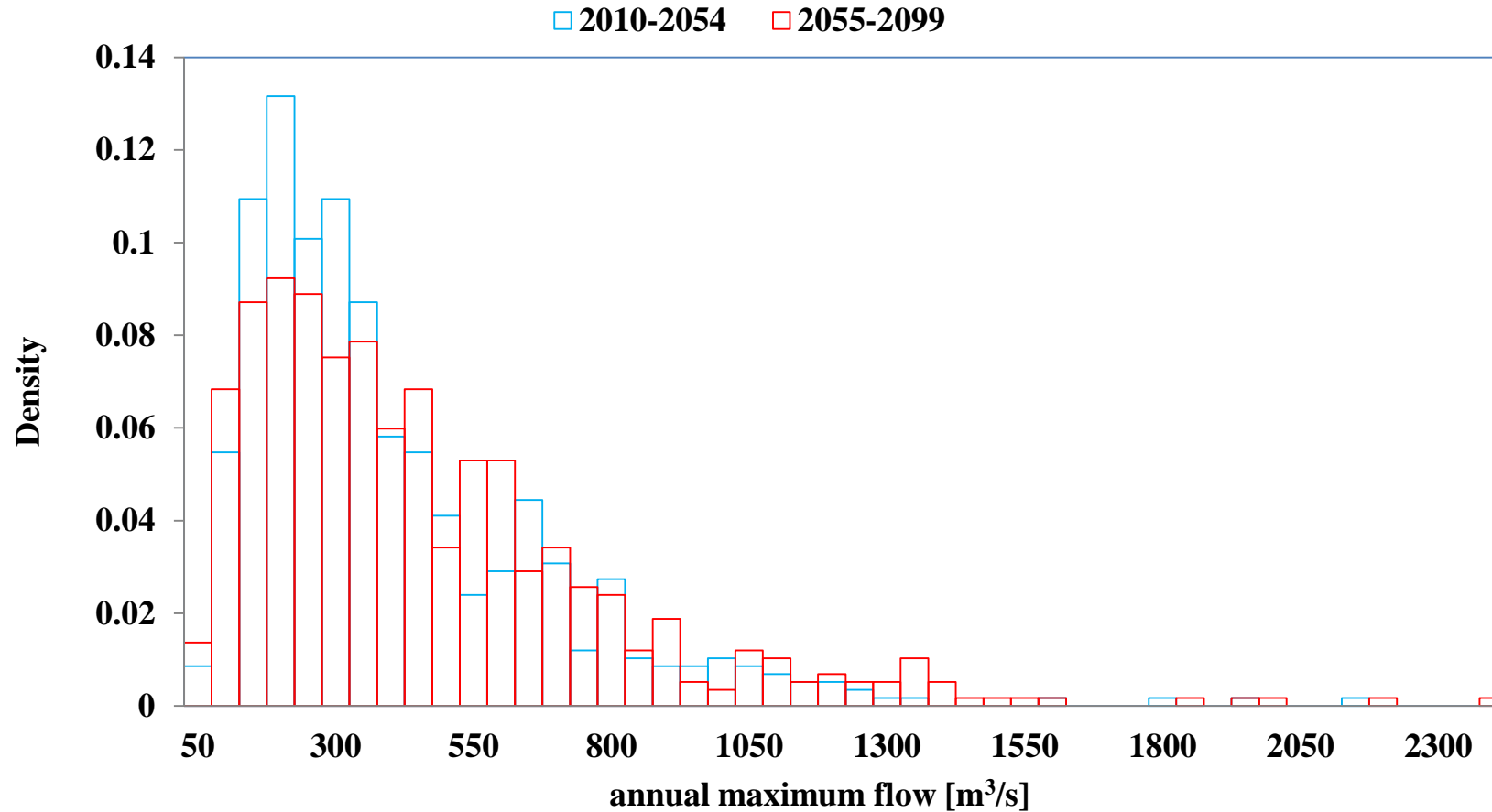
Comparison of the flood frequency curve at Yolo station
using observed flows (1903-2012),
with the curve estimated by the WEHY model-simulated flows based on the
downscaled GCM historical control run simulations



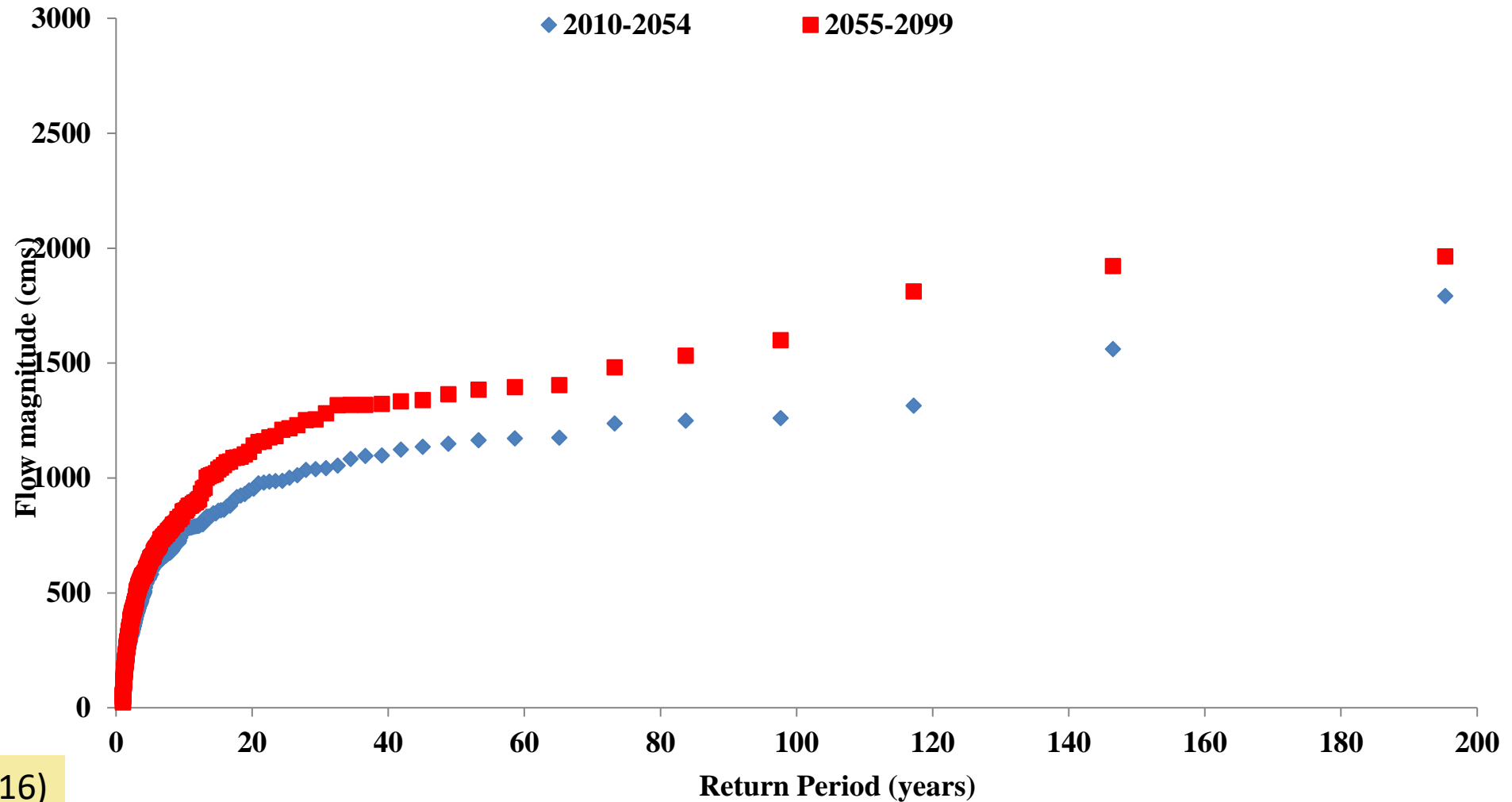
Annual maximum model-simulated streamflows during 21st century at Yolo gauging station



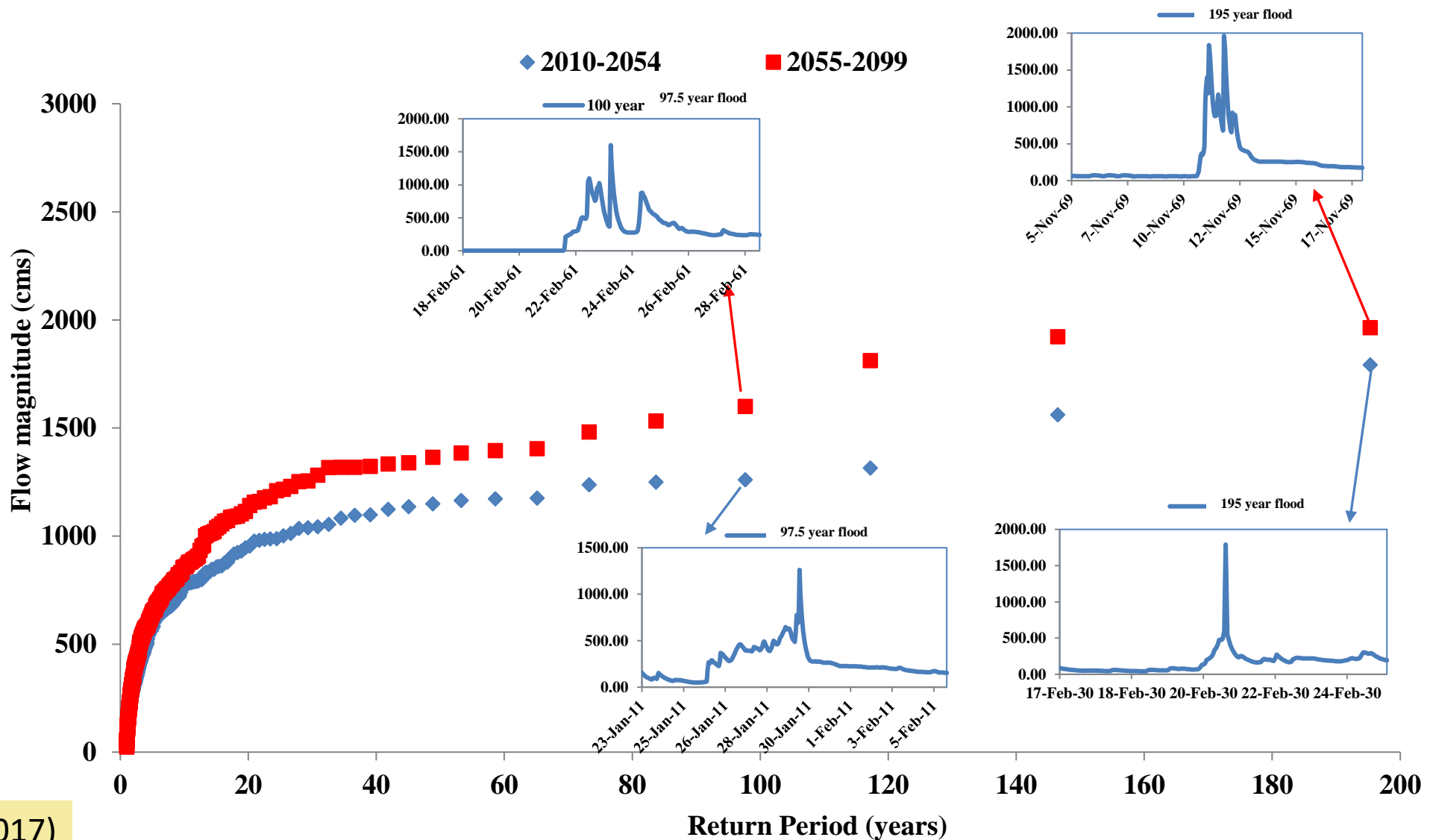
Relative frequency histograms of annual maximum flows separated into 45-year increments for all flow projections during 21st century at Yolo gauging station



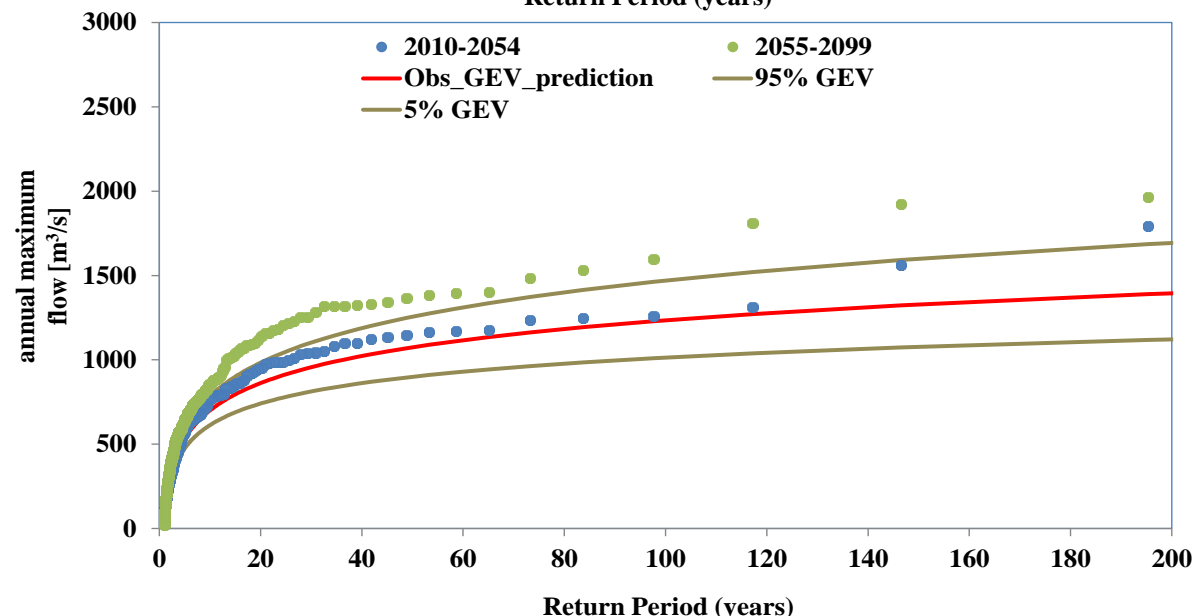
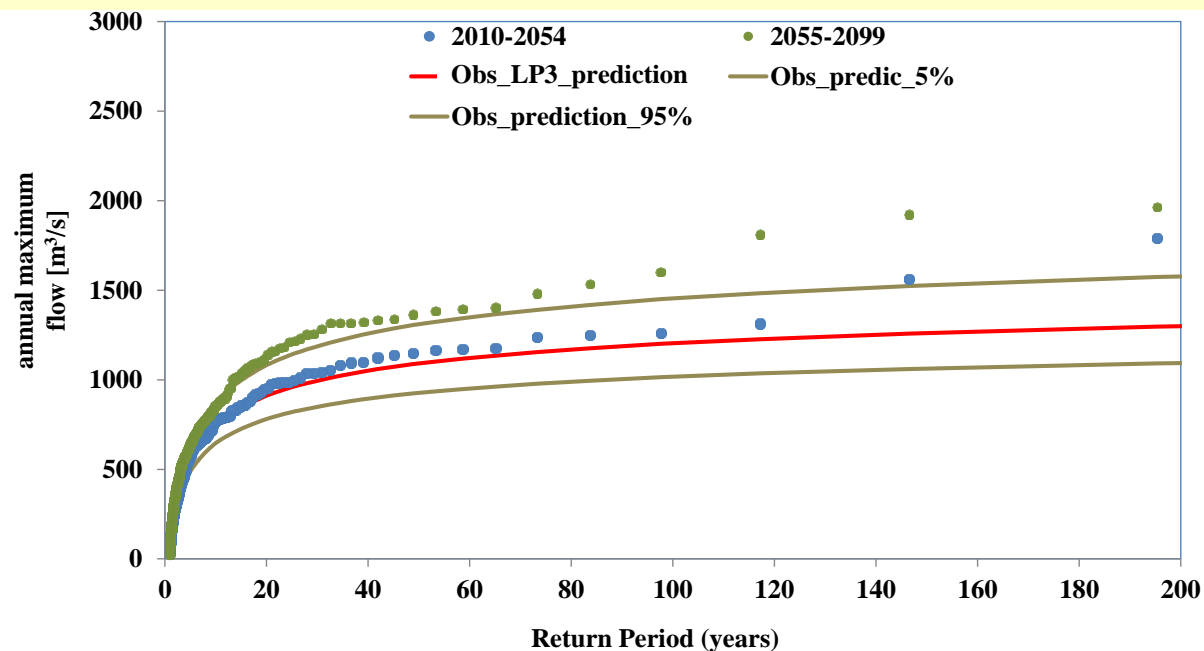
Evolution of the annual maximum flow as function of return periods throughout the 21st century for all flow projections at Yolo gauging station



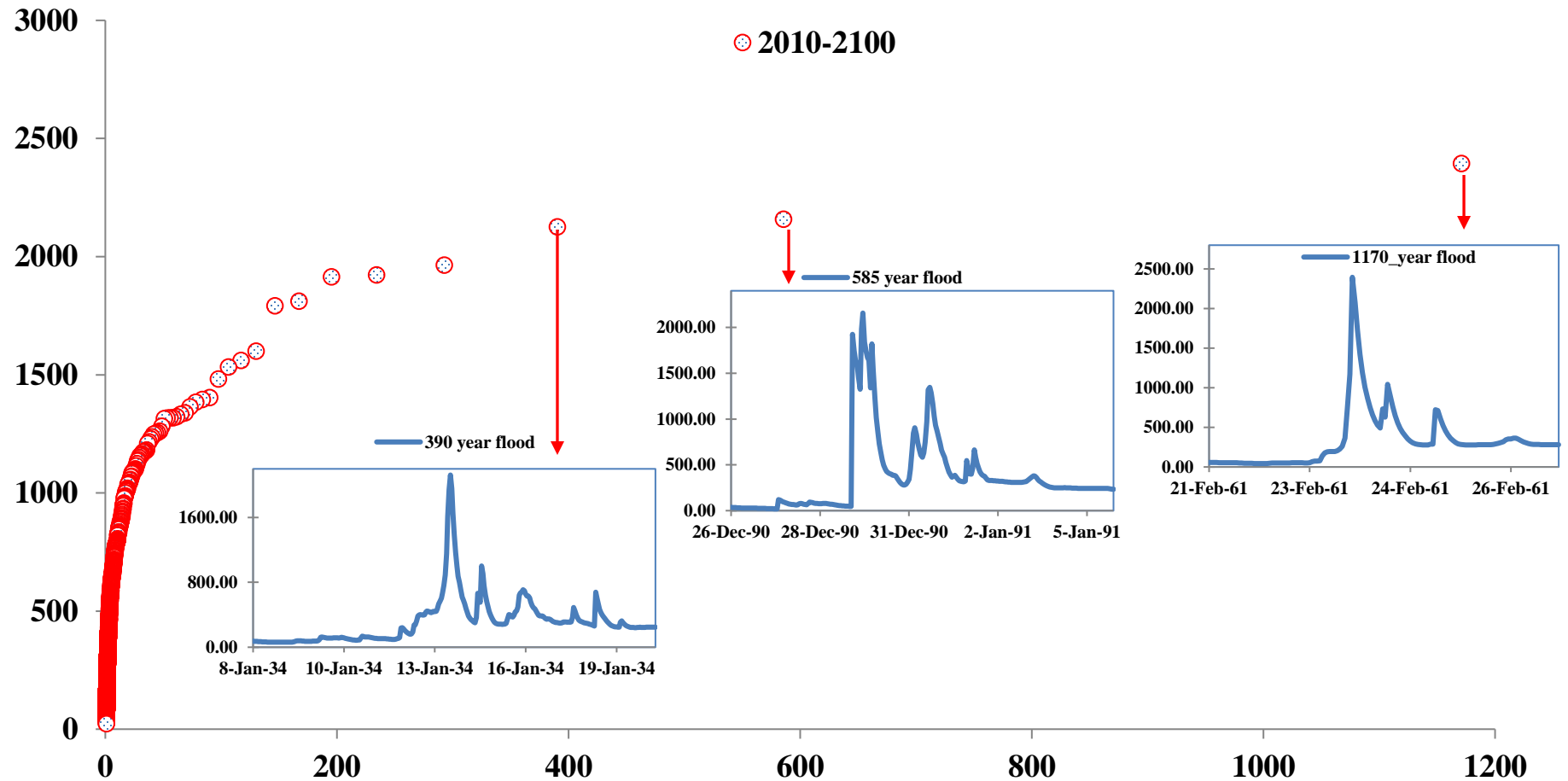
Evolution of the annual maximum flow as function of return periods throughout the 21st century for all flow projections at Yolo gauging station



Comparison between Fitted LP3 and GEV distributions that were calibrated by historical observations, against hydroclimate simulations-based distributions during two periods of future projection



Annual maximum flow as function of return period throughout the 21st century for all flow projections at Yolo gauging station



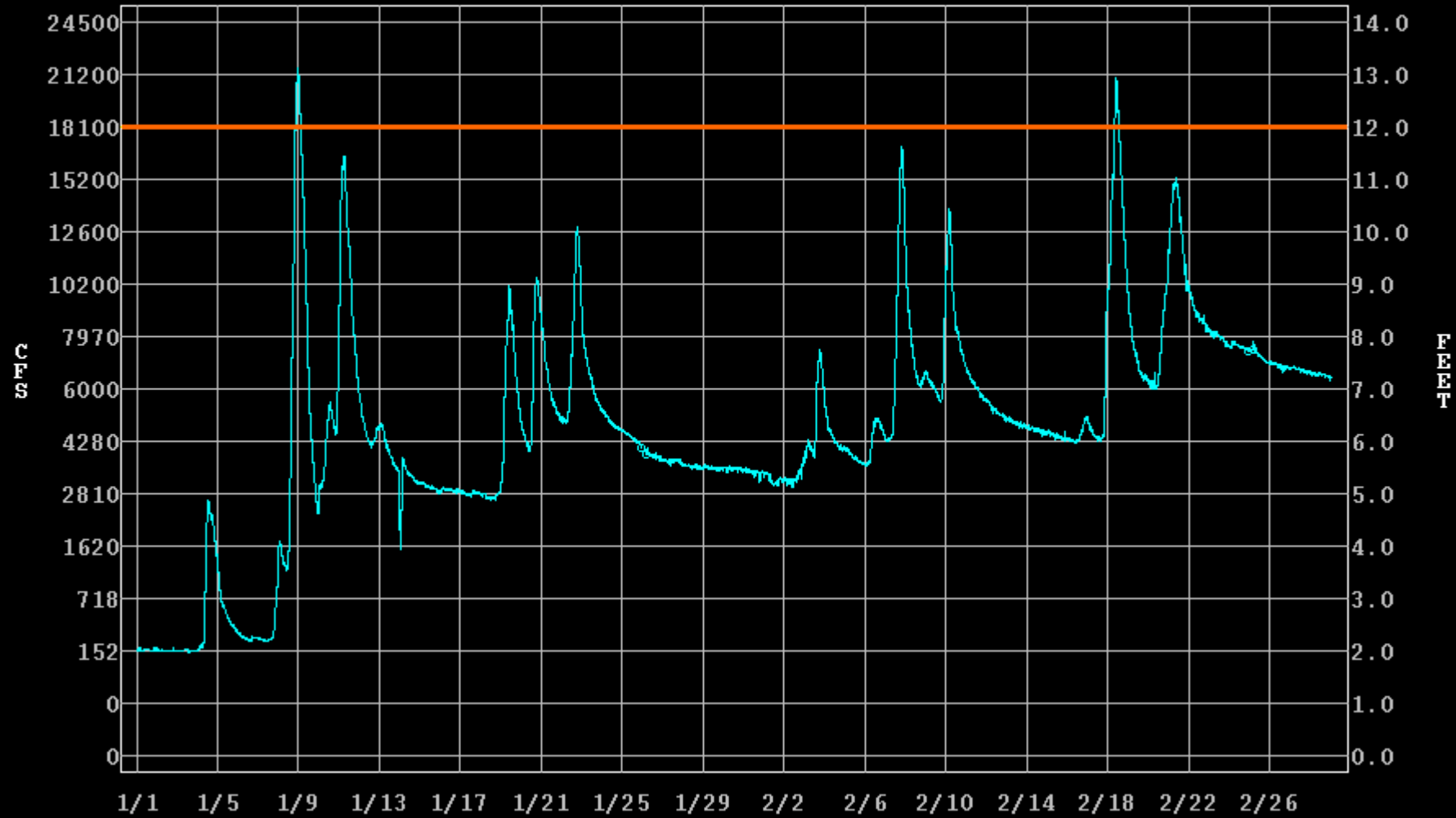
Cache Creek - Rumsey (RMSC1)

River Stage / Flow Plot

Maximum Value: 13.1 Feet / 21,550 cfs (January 8, 2017 at 23 UTC)

Monitor Stage: 12.0 Feet

Flood Stage: 14.0 Feet



SELECTED REFERENCES

- Cowpertwait, S.P., 1998. "A Poisson Cluster Model of Rainfall: Higher Order Moments and Extreme Values", Royal Society Proceedings: Mathematical, Physical and Engineering Sciences , Mar. 8, 1998, Vol. 454, No. 1971, pp. 885-898
- Hershfield, D. M. 1961. "Estimating the probable maximum precipitation." J. Hydraul. Div. 87 (5): 99–116.
<https://doi.org/10.1061/JYCEAJ.0000651>
- Hiraga, Y.; Yoshihiko Iseri; Michael D. Warner; Chris D. Frans; Angela M. Duren; John F. England; M. Levent Kavvas
Comparison of Numerical Weather Model-based Precipitation Maximization methods: Moisture optimization method, Storm transposition method, and their combination. Journal of Hydrologic Engineering, Ms. No. HEENG-5781R2, Aug. 2022.
- Iseri, Y., A. J. Diaz, T. Trinh, M. L. Kavvas, K. Ishida, M. L. Anderson, N. Ohara, and E. D. Snider. 2021. "Dynamical downscaling of global reanalysis data for high-resolution spatial modeling of snow accumulation/melting at the central/southern Sierra Nevada water-sheds." J. Hydrol. 598 (Jul): 126445.
- Ishida, K., M. L. Kavvas, S. Jang, Z. Q. Chen, N. Ohara, and M. L. Anderson. 2015. "Physically based estimation of maximum precipitation over three watersheds in Northern California: Atmospheric boundary condition shifting." J. Hydrol. Eng. 20 (Apr): 04014052. [https://doi.org/10.1061/\(ASCE\)HE.1943-5584.0001026](https://doi.org/10.1061/(ASCE)HE.1943-5584.0001026).
- Ishida, K., M. L. Kavvas, Z. Q. R. Chen, A. Dib, A. J. Diaz, M. L. Anderson, and T. Trinh, 2018. "Physically based maximum precipitation estimation under future climate change conditions", Hydrol. Process., 32, 3188–3201, doi:10.1002/hyp.13253.
- Kavvas, M. L., Kure, S., Chen, Z. Q., Ohara, N., & Jang, S. (2013). WEHY-HCM for modeling interactive atmospheric-hydrologic processes at watershed scale. I: Model description. J. of Hydrologic Engineering, 18(10), 1262–1271.
- Kavvas, M. L., Y. Iseri, Y. Hiraga, K. Toride, "Atmospheric Modeling to Predict Risks to Dams from Extreme Rainfall Events at Columbia River Basin". Final Project Report, submitted to US Corps of Engineers, Dec. 2021.
- Kavvas, L., Y. Iseri, Y. Hiraga, A. Duren, J. England, C. Frans, M. Warner, "Maximum Precipitation Approach for the Columbia River Basin Dams", USACE Publication, March, 2023.

- Hiraga, Y., Iseri, Y., Warner, M.D., Frans, C.D., Duren, A.M., England, J.F., Kavvas, M.L. 2021. Estimation of Long-duration Maximum Precipitation during a winter season for large basins dominated by Atmospheric Rivers using a Numerical Weather Model. *J. Hydrol.* 598, 126224. <https://doi.org/10.1016/j.jhydrol.2021.126224>.
- Kavvas, M. L., T. Trinh, K. Ishida, I. Fisher, S. Jang, J. Nosacka and K. Brown, 2016. “Estimation of Flood Frequencies under Changing Climate Conditions During 21st Century by means of a Numerical Coupled Atmospheric-Hydrologic Modeling Approach”, Invited Lecture at 2017 AGU Fall Meeting.
- Mure-Ravaud, M., A. Dib, M. L. Kavvas, and E. Yegorova, 2018, “Maximization of the precipitation from tropical cyclones over a target area through physically based storm transposition”, *HESS*, <https://doi.org/10.5194/hess-2017-665>
- Ohara, N., M. L. Kavvas, S. Kure, Z. Q. Chen, S. Jang, and E. Tan. 2011. “Physically based estimation of maximum precipitation over American River Watershed, California.” *J. Hydrol. Eng.* 16 (4): 351–361. [https://doi.org/10.1061/\(ASCE\)HE.1943-5584.0000324](https://doi.org/10.1061/(ASCE)HE.1943-5584.0000324).
- Ohara, N., & Kavvas, M. L. (2006). Field observations and numerical model experiments for the snowmelt process at a field site. *Advances in Water Resources*, 29(2), 194–211.
- Toride, K., Y. Iseri, M. D. Warner, C. D. Frans, A. M. Duren, J. F. England, and M. L. Kavvas. 2019. “Model-based probable maximum precipitation estimation: How to estimate the worst-case scenario induced by atmospheric rivers?” *J. Hydrometeorol.* 20 (12): 2383–2400.
- Trinh, T.Q.; K. Ishida, I. Fischer, S-H Jang, J. Nosacka, K. Brown, Y. Darama, M.L. Kavvas, “New Methodology to Develop Future Flood Frequency under Changing Climate by Means of Physically-based Numerical Atmospheric-Hydrologic Modeling *Journal of Hydrologic Engineering*, Vol. 21, No. 4.: 04016001, 2016
- Trinh, T., Iseri, Y., Diaz, A., Snider, E., Anderson, M., Kavvas, M.L. : Maximization of historical storm events over seven watersheds in central/southern Sierra Nevada by means of Atmospheric Boundary Condition shifting and relative humidity optimization methods, *Journal of Hydrologic Engineering*, Vol. 27, No. 3, 04021051, March 2022.
- Trinh, T., A. Diaz, Y. Iseri, E. Snider, M.L. Anderson, K.J. Carr, M.L. Kavvas, A numerical coupled atmospheric-hydrologic modeling system for probable maximum flood estimation with application to California's Southern Sierra Nevada foothills watersheds, *Journal of Flood Risk Management*, e12809., April 2022, <https://doi.org/10.1111/jfr3.12809>.
- WMO (World Meteorological Organization). 2009. *Manual on estimation of probable maximum precipitation (PMP)*. WMO-1045. Geneva: WMO.

THANK YOU